Impacts of physical parametrization on prediction of ethane concentrations for oil and gas emissions in WRF-Chem

Maryam Abdi-Oskouei[1], Gabriele Pfister[2], Frank Flocke[2], Negin Sobhani[2], Pablo Saide[3], Alan Fried[4], Dirk Richter[4], Petter Weibring[4], and James Walega[4], Gregory Carmichael[1]

[1] Center for Global and Regional Environmental Research (CGRER), University of Iowa, Iowa City, Iowa, USA
[2] National Center for Atmospheric Research (NCAR), Boulder, Colorado, USA
[3] Department of Atmospheric and Oceanic Sciences, University of California Los Angeles (UCLA), Los Angeles, California, USA
[4] Institute of Arctic and Alpine Research, University of Colorado, Boulder, CO, USA

Correspondence to: Maryam Abdi-Oskouei (maryam-abdioskouei@uiowa.edu)

Abstract. Recent increases in the Natural Gas (NG) production through hydraulic fracturing have called into question the climate benefit of switching from coal-fired to natural gas-fired power plants. Higher than expected levels of methane, Non-Methane Hydrocarbons (NMHC), and NOx have been observed in areas close to oil and NG operation facilities. Large uncertainties in the oil and NG operation emission inventories reduce the confidence level in the impact assessment of such activities on regional air quality and climate, as well as development of effective mitigation policies. In this work, we used ethane as the indicator of oil and NG emissions and explored the sensitivity of ethane to different physical parametrizations and simulation set-ups in the Weather Research and Forecasting with Chemistry (WRF-Chem) model using the U.S. EPA National Emission Inventory (NEI-2011). We evaluated the impact of the following configurations and parameterizations on predicted ethane concentrations: Planetary Boundary Layer (PBL) parametrizations, daily re-initialization of meteorological variables, meteorological initial and boundary conditions, and horizontal resolution. We assessed the uncertainties around oil and NG emissions by using measurements from the FRAPPÉ and DISCOVER-AQ campaigns over the Northern Front Range Metropolitan Area (NFRMA) in summer 2014. The sensitivity analysis shows up to 57.3% variability in normalized mean bias of the near-surface modeled ethane across the simulations, which highlights the important role of model configurations on the model performance and ultimately the assessment of emissions. Comparison between airborne measurements and the sensitivity simulations indicates that the model-measurement bias of ethane ranged from -14.9 ppb to -8.2 ppb (NMB ranged from -80.5% to -44%) in regions close to oil and NG activities. Under-prediction of ethane concentration in all sensitivity runs suggests an actual under-estimation of the oil and NG emissions in the NEI-2011. Increase of oil and NG emissions in the simulations partially improved the model performance in capturing ethane and lumped alkanes (HC3) concentrations but did not impact the model performance in capturing benzene, toluene, and xylene which is due to very low emission rates of these species from oil and NG sector in the NEI-2011.

1. Introduction

Recent advances in the unconventional Natural Gas (NG) production technology (hydraulic fracturing) have resulted in economical access to NG reserves in deep shale formations and a 36% rise in US NG production from 2005 to 2014 (Lyon, 2015). Increase in the NG production, decrease in the NG price, and environmental advantages of NG-fired power plants over coal-fired power plants have made NG an important competitor for coal in the electricity generation sector. In 2015, NG and coal each had a 33% share in the electricity generation in the US. It is predicted that NG's share in electricity generation will grow 1.5% every year (Energy information administration of US Department of Energy., 2016; U.S. Energy Information Administration, 2016). With the rapid increase in the unconventional oil and NG production, higher than expected levels of greenhouse gases, specifically methane, and air pollutants such Non-Methane Hydrocarbons (NMHC) and NO_x (from flaring or compressors, reboilers, pneumatic devices, trucks, and other equipment using fossil fuel) (Allen, 2016; Olaguer, 2012) have been observed in some places in vicinity of oil and NG facilities. The high concentrations of these chemicals measured in many studies at different scales and regions suggest that official emission inventories (e. g. Greenhouse Gas Inventory (GHGI) and Emission Database for Global Atmospheric Research (EDGAR)) fail to capture the magnitude of emissions from unconventional extraction activities (Brandt et al., 2014). The underestimation of emission inventories has raised concerns regarding the climate implications of promoting NG as the "bridge fuel" (Alvarez et al., 2012; Howarth et al., 2011; Levi, 2013; McJeon et al., 2014), and its impacts on the air quality and public health (Halliday et al., 2016; McKenzie et al., 2012). Additionally, Methane and NMHC emitted from the oil and NG sector can degrade regional air quality and contribute to ozone formation on regional and global scales (Helmig et al., 2016). Outdated Emission Factors (EF), super-emitters in the production systems, and rapid growth in the production facilities are some of the reasons for the underestimation (Brandt et al., 2014; Lyon, 2015; Zavala-Araiza et al., 2015).

The Colorado Northern Front Range (NFR), including the Denver metropolitan area, is located between the Rocky Mountains and the High Plains with a total population of about 4.8 million. In 2007, a large region of the NFR was declared in nonattainment of the National Ambient Air Quality Standard (NAAQS) for 8h average ozone. Major sources of pollutants in this area are vehicle emissions, oil and NG operation, agriculture and feedlots, and power plants. In the past years, oil and NG development has increased drastically in the NFR. NG production in Weld County has increased from 55.8×10^6 m^3 (1.97×10^6 Thousand Cubic Feet (MCF)) to 181.8×10^6 m^3 (6.42×10^6 MCF) from 2004 to 2016. The Wattenberg gas field in Weld County is close to populated regions and has the highest well density in the NFR with more than 25,000 active NG wells (Colorado Oil and Gas Conservation Commission, 2017). In the NFR, measured NMHCs are 18-77 times greater than the regional background as determined from the NOAA flask network (Thompson et al., 2014). High levels of NMHC can cause health concerns at regional scales and can contribute significantly to the ozone pollution in the region (Cheadle et al., 2017; Gilman

et al., 2013; McDuffie et al., 2016; Pétron et al., 2012; Pfister et al., 2017b; Thompson et al., 2014). Using box models constrained with observations, McDuffie et al. (2016) estimated that NFR oil and NG activities contribute ~50% to the regional Volatile Organic Compound (VOC) OH reactivity and 20% to the regional photochemical ozone production.

5   Mass balance approach methods have been widely used to estimate the emissions from oil and NG activities (Conley et al., 2016; Karion et al., 2015; Peischl et al., 2016; Pétron et al., 2012; Smith et al., 2015). This method cannot provide details on the spatial and temporal variability of emissions and has limitations in domains with complex atmospheric transport such as the NFR. High resolution three-dimensional atmospheric chemical transport models can better capture the variability in meteorology and chemistry in different domains. Paired with observations and using inverse modeling techniques, these
10   models help evaluate the performance of emission inventories on high temporal and spatial scales (Barkley et al., 2017; Cui et al., 2014, 2017) and allow assessments of the impact of oil and NG activities on regional air quality. Ahmadov et al. (2015) used the Weather Research and Forecasting Model with Chemistry (WRF-Chem) to study high ozone episodes and emission reduction scenarios in the Uintah Basin. Their results show a strong underestimation of methane and VOC emissions in the National Emission Inventory 2011 (NEI-2011).

WRF-Chem provides users with different dynamical, physical, and chemical schemes (Grell et al., 2005; Skamarock et al., 2008). These choices can impact the performance of the model, specifically in regions with complex transport patterns (Saide et al., 2011). In order to assess the performance of emission inventories, it is critical to address the uncertainties derived from model configurations on simulated concentration fields. The goal of this study is to quantify the impact of WRF-Chem
20   configurations on predicting the oil and NG emissions in the NFR. VOCs in the NFR have shown a clear source signature associated with oil and NG activities (Gilman et al., 2013; Pétron et al., 2014). Diverse air pollution sources and complex metrological patterns due to mountain-valley circulation, high elevation, and harsh terrain are some of the challenges for air quality modeling in this area. We use ethane, which has a simple chemical cycle and a lifetime of about two months, as a tracer for oil and NG (Helmig et al., 2016). The model and emission inventory performance are evaluated by comparing
25   meteorological parameters as well as ethane and VOC concentrations to surface and airborne measurements. We explore the sensitivity of the modeled transport and ethane concentrations to different WRF-Chem physical parametrizations and set-ups. This work will be followed by development of an inverse modeling technique to constrain the oil and NG emission rates by calculating optimal scaling factor for the emission inventory. Simulations discussed in this study will be used to calculate the variability of the optimal scaling factor. To inform not only about the absolute magnitude in the ethane emissions but to further
30   explore the feasibility to constrain other trace gas oil and NG emissions, we investigate CO and VOC emission estimates from oil and NG sector and VOC ratios in the observations and the model.

2. Method

2.1. Aircraft and ground-based observations

The National Science Foundation/National Center for Atmospheric Research (NSF/NCAR) Front Range Air Pollution and Photochemistry Éxperiment (FRAPPÉ) and National Aeronautics and Space Administration (NASA) Deriving Information on Surface Conditions from COlumn and VERtically Resolved Observations Relevant to Air Quality (DISCOVER-AQ) campaigns were conducted in July and August 2014, in the NFR Colorado. These two campaigns provide detailed and coherent airborne and ground-based measurements in this area, which can assist in evaluation and improvement of chemical transport models and emission inventories. The NSF/NCAR C130 collected extensive airborne measurements of various atmospheric constituents during the FRAPPÉ campaign. A total of 15 flights (~80 flight hours) were conducted in the NFR with the goal of mapping the emissions and their transport and chemistry in this region. During the DISCOVER-AQ campaign, the NASA P3B aircraft performed approximately 20 flights containing spiral ascents or descents over six key sites in the NFR to capture the vertical profiles of the atmospheric constituents and their diurnal variation. Ethane was measured on board of C130 and P3 aircrafts. On C130 aircraft, ethane was measured by the University of Colorado's CAM instruments with detection sensitivity of 15 ppt, details for which are discussed in Richter et al. (2015). Aerodyne Ethane-Mini spectrometer on P3 was used to measure ethane concentration (Yacovitch et al., 2014). Fried (2015) compared CAMS ethane measurements with sub-ppb precision with the Aerodyne measurements during wing tip comparisons and the agreement was within 9%, corresponding to differences of less than 55 ppt.

The National Oceanic and Atmospheric Administration (NOAA), the Colorado Department of Public Health and Environment (CDPHE), and the National Park Services (NPS) operated numerous ground-level measurement sites during these two campaigns. In this work, we present ground-level measurements from the NOAA Boulder Atmospheric Observatory (BAO; 40.05°N, 105.01°W, 1584 m above sea level (asl)), the NOAA Platteville site (PAO; 40.18°N, −104.73°W, 1523 m asl), Fort Collins (FC; 40.89°N, -105.13°W, 1572 m asl), NREL-Golden (Golden; 39.74°N, -105.18°W, 1833 m asl), and CDPHE wind measurements at Weld County tower (WC-Tower; 40.39°N, -104.73°W, 1483 m asl), Rocky Flats N (RF-N;39.91°N, -105,19°W, 1803 m asl), Welch (39.64°N, -105.14°W, 1743 m asl), Chatfield (39.53°N, -105.07°W, 16756 m asl), and Aurora-East (39.64°N, -104.57°W, 1802m asl). BAO and PAO are located north of Denver and close to the Wattenberg Gas Field in Weld County (Figure 1). Measurements of temperature, relative humidity, wind speed and direction at 10m, 100m, and 300m were recorded at BAO. Surface wind measurements from PAO (3m) and WC-Tower (4m) were used in this study. The planetary Boundary Layer (PBL) height was measured and calculated at PAO, Fort Collins (FC), and NREL-Golden using micro-pulse Lidar backscatter during the daytime (Compton et al., 2013).

2.2. WRF-Chem model

We used WRF-Chem 3.6.1 (Grell et al., 2005; Skamarock et al., 2008), a fully coupled online air quality and transport model, to investigate the sensitivity of modeled PBL, winds, temperature, relative humidity, and ethane concentrations to different

physical parametrizations and configurations. Figure 1 illustrates the location of the two nested domains and the underlying terrain map. We used one-way nesting (i.e., the outer domain ran independently of the inner domain). The outer domain has a 12 km × 12 km horizontal resolution, and the inner domain has a 4 km × 4 km horizontal resolution. Both domains have 53 vertical levels with the domain top at 50 hPa (~11 layers below 1km). The outer domain is designed to capture the emission

5   from the Western US, and the inner domain includes Colorado and Utah. Sensitivity simulations start on 24 July 2014 and end on 18 Aug 2014. Table 1 shows a summary of the WRF-Chem configurations for this study, used in all sensitivity simulations. The Morrison double-moment scheme was selected as the microphysics option and Goddard shortwave (Chou and Suarez, 1999) and RRTMG longwave radiation schemes (Iacono et al., 2008) were used as shortwave and longwave radiation parametrizations, respectively. The Grell-Freitas convection scheme (Grell and Freitas, 2014) was used as convective

10   parametrization for both outer and inner domain. The inner domain falls into the "grey-scale" which means many of the assumptions used in convective parametrization will no longer be valid at this resolution. The Grell-Freitas convection scheme is a stochastic scale dependent convective parametrization based on the method proposed by Arakawa et al. (2011) and is designed for domains with horizontal resolution up to few kilometers. Comparisons between a simulation with resolved convection of inner domain and a simulation using the Grell-Freitas convective parametrization in the inner domain showed

15   similar performance in capturing transport (not shown). Thus, we used the Grell-Freitas convective scheme for both domains in all simulations to reduce the computation costs.

We selected the Regional Atmospheric Chemistry Mechanism chemistry using Earth System Research Laboratory (RACM-ESRL) (Stockwell et al., 1997) coupled to the Modal Aerosol Dynamics Model/Secondary Organic Aerosol Model (MADE/SORGAM). RACM includes 17 stable inorganics, 4 inorganic intermediates, 32 stable organic species, and 24 organic

20   intermediates. RACM_ESRL (Kim et al., 2009) is an updated version of the RACM mechanism and includes 23 photolysis and 221 chemical reactions (Ahmadov et al., 2015). To reduce the computational costs, hydrocarbons with similar behavior are lumped together in the chemical mechanisms. For example, "HC3" in the RACM_ESRL mechanism includes alkanes such as propane, n-butane, isobutane, and acetylene (ethyne), and alcohols such as methanol and ethanol. "TOL" includes toluene and benzene. Ethane and methane are treated exclusively in the RACM_ESRL mechanism. More details regarding the

25   reactions and lumping groups can be found in Stockwell et al., 1997. Chemical boundary conditions from Monitoring Atmospheric Composition and Climate reanalysis (MACC), available every 3 hours, (Inness et al., 2013) and model outputs from RAQMS, available every 6 hours, (Natarajan et al., 2012; Pierce et al., 2007) were used as chemical boundary and initial conditions in the simulations. The model outputs from these global models are specific to the simulation time (24 July 2014 tp 18 Aug 2014) and are interpolated to the WRF-Chem domain and temporal resolution prior to starting the simulations. Ethane

30   concentrations showed no strong sensitivity to the two different chemical initial and boundary conditions (i.e., RAQMS and MACC) and is not discussed further.

2.2.1.   WRF-Chem sensitivity tests

WRF-Chem provides users with a number of different dynamical, physical, and chemical schemes. Users can select schemes based on the physical properties of the domain of interest, goals of the study, and computational limitations. We evaluated the

sensitivity of WRF-Chem to different physics options, such as the PBL parametrization, and configurations including daily re-initialization of meteorological fields, different meteorological initial and boundary conditions, and varying horizontal resolution. Table 2 shows details on the sensitivity runs and lists the meteorological and chemical boundary conditions used for each run. The naming system for the simulations is based on the different settings (e.g. simulation 5-MnERi represents the simulation number (5), PBL Scheme (MYNN3), meteorological initial and boundary condition (ERA-interim), chemical initial and boundary condition (RAQMS), and daily re-initialization of meteorological fields (i)). Simulation ID in Table 2 has been used when discussing sensitivity tests in the paper.

An accurate simulation of air pollution is dependent on a precise description of transport processes, meteorological conditions, and the PBL height (PBLH) (Cuchiara et al., 2014; Hu et al., 2010; Sobhani et al., 2018). Transport of pollutants within the domain depends on turbulent motions and vertical mixing within the PBL. WRF-Chem (3.6.1) has eleven different PBL schemes to address the closure problem in the simulation of turbulent motions. In general, PBL schemes can be classified into two main groups; local and non-local. A local PBL scheme estimates the turbulent fluxes of heat, momentum, and moisture from local mean and gradient flux values. In a non-local PBL scheme, non-local fluxes can influence fluxes in each grid, hence they are expected to better capture large-size eddies in the simulation (Stull, 1988). We tested one non-local and two local PBL schemes to understand the sensitivity of the model to PBL parameterization in a domain with high elevation and complex terrain. We used Yonsei University (YSU) first order (Hong et al., 2006) as the non-local PBL scheme in the PBL1 (1-YFM) simulation. The local schemes used in PBL2 (2-MjFM) and PBL3 (3-MnFM) simulations were Mellor–Yamada–Janjic (MYJ) 1.5 order (2.5 level) (Janjic, 2001; Janjic et al., 2000) and Mellor-Yamada-Nakanishi-Niino (MYNN3) 3rd level (Nakanishi and Niino, 2009).

WRF-Chem is a mesoscale model and requires initial and lateral boundary conditions from a larger-scale model. Usually, these initial and lateral boundary conditions are taken from re-analysis products of larger-scale models optimized using assimilation techniques and observations. The choice of initial and lateral boundary condition products can impact the model performance (Angevine et al., 2012; Saide et al., 2011). We tested two different meteorological initial and boundary conditions, European Reanalysis (ERA-interim) by European Center for Medium-Range Weather Forecasts (ECMWF) in Met5 (5-MnERi) simulation and NCEP's Global Forecast System (GFS) in Met6 (6-MnFRi) simulation. ERA-Interim reanalysis is produced with 80km by 80km horizontal and 6-hour temporal resolution (European Centre for Medium-Range Weather Forecasts (ECMWF), 2009), and NCEP FNL (final) operational global analysis is produced using GFS with 1-degree by 1-degree horizontal and 6-hour temporal resolution (National Centers for Environmental Prediction, National Weather Service, NOAA, 2000).

Simulations were performed for 24 days from 24 July 2014 to 18 August 2014. Initializing the meteorological fields in the simulation at the first time step with the larger-scale model values and running it for 24 days without any nudging will result

in deviations from the larger scale re-analysis products. On the other hand, the lower resolution of the larger-scale models can lower the accuracy of WRF-Chem high-resolution simulations. To investigate this impact, we tested two different set-ups for WRF-Chem. In Init4 (4-MnER) simulation, we initialized the meteorological fields at the first time step with larger-scale model values and ran the simulation freely for 24 days ("free run"). In Init5 (5-MnERi) simulation, the meteorological fields were re-initialized every day at 18 UTC (12pm local time) and run for the next 30 hours. The first 6 hours of the simulation (18 UTC to 00 UTC) were discarded to allow for the model to spin up. In this set-up, chemistry fields were recycled from previous cycles of simulations.

The sensitivity of the model to the horizontal resolution was examined by comparing the performance of the outer domain (12 km × 12 km) to the inner domain (4 km × 4 km) in Hor5 (5-MnERi) simulation. In one-way nesting, the outer domain runs independently of the inner domain; thus, comparing the performance of the outer and inner domains is valid.

2.3. Emission inventory

NEI-2011 version 2 is a bottom-up emission inventory of U.S. anthropogenic emissions. While we cannot expect the year 2011 inventory to fully represent the model year 2014, it was the only inventory available to the WRF-Chem user community at the time of this study. Emissions in this inventory are calculated based on fuel consumption, source activity, and emission factors reported by state, tribal, and local governing agencies (U.S. Environmental Protection Agency, 2015). A processed version of NEI-2011 is available to the users, which includes emission of 76 species (50 speciated VOC compounds, 19 PM2.5 aerosol species, and 7 primary species). NEI-2011 and emissions for only oil and NG sector in the NEI-2011 were provided to us by Dr. Stuart McKeen (NOAA Earth Systems Laboratory, Boulder, CO). Table SM 1 includes details on the mapping table used to convert NEI-2011 species to RACM and MADE/SORGAM chemical and aerosol mechanism. The separate oil and NG emission information was used to conduct an additional sensitivity simulation with perturbed oil and NG emission, which we used to study the sensitivity of modeled ethane concentrations as well as concentrations of VOCs and CO to the oil and NG emission sector. We used the Model of Emissions of Gases and Aerosols from Nature (MEGAN) for biogenic emission in all simulations (Guenther et al., 2012). Ethane does not have a significant biogenic source (Yacovitch et al., 2014); thus, we did not assess the impact of biogenic emissions in this study. Wildfire emissions were not included in the simulations, but this will have a negligible impact on the results as wildfires did not significantly influence the air quality in the NFR during the FRAPPÉ campaign (Valerino et al., 2017).

3. Results and Discussion

We start with an evaluation of the overall performance of all simulations and later provide a detailed discussion on the different sets of sensitivity simulations. To evaluate the sensitivity of WRF-Chem to different physical parametrizations, we compared the simulated meteorological variables, such as temperature, relative humidity, wind fields, and PBLH, with measurements.

27 July 2014 and 28 July 2014 were reported as Denver cyclone episodes (Dingle et al., 2016; Valerino et al., 2017; Vu et al., 2016), and neither simulation captured the cyclone pattern and enhancements accurately on these two days. Thus, we only included the period of 1 August 2014 to 15 August 2014 in our analysis to avoid skewing the results because of large model errors during the Denver cyclone episode. For quantitative comparison between the simulations, we used statistical measures

5   including correlation coefficient (R), root mean square error (RMSE), mean absolute error (MAE), mean bias (MB), and normalized mean bias (NMB). Definitions of these metrics can be found in the supplement. We used NMB as a proxy for model sensitivity to quantify the impact of model configuration on different variables. Variability of NMB (calculated by subtracting minimum NMB from maximum NMB) in sensitivity tests can provide a range for uncertainties in the model cases independent of the model values.

3.1.   Evaluation of overall model performance

Table 3 includes the statistical measures for temperature and relative humidity in all the simulation tests at 100m altitude at BAO. Figure 2 compares the diurnal cycles of measured temperature, relative humidity, wind speed, and wind direction at 100m altitude at BAO with corresponding model values for all the simulation tests. While Figure 2 provides an overview of

15   all sensitivity tests, Figure SM 2 separates each sensitivity test to provide a clearer test by test comparison. Similarly, Table SM 2 to 5 includes statistical measures and Figure SM 1 and Figure SM 3 show diurnal cycles of temperature, relative humidity, wind speed, and wind direction at BAO 10m and 300m. All model simulations capture the overall daily cycle in temperature and relative humidity well (Figure 2 and Table 3). The variability across different sensitivity runs can be large, with modeled temperature varying by up to 6°C and the model-measurement NMB ranging from -3.9% to 11.1%. Relative humidity has

20   larger variability among the simulations during nighttime compared to daytime. The NMB of relative humidity ranges from -29.7% to 52.6%.

Wind patterns vary significantly from daytime to nighttime. During the day, wind primarily blows from the east towards the Rocky Mountains with a slight southerly component. During the night, this pattern switches to predominantly westerly winds

25   bringing cooler air to lower terrain. Wind measurements at the BAO at different altitudes (10m, 100m, 300m) can help us better understand the wind pattern at higher model levels. Table 4 includes mean and standard deviation of daytime and nighttime wind fields in the simulations and the observations at 100m. Results for the 10m and 300m level at BAO during 1 August 2014 to 15 August 2014 are included in Table SM 4 and Table SM 5, respectively. In addition to BAO, we investigated the wind sensitivity to physical parametrizations at two other sites that are close to oil and NG operations, WC tower and PAO

30   (Figure SM 5). At BAO, higher wind speeds were measured at higher elevations which is captured by the model. Overall, most simulations show skill in capturing diurnal cycles of wind speed and direction with better agreement with observations for daytime (Table 4, Table SM 4, and Table SM 5). Overall, the model runs show fairly good performance in capturing temperature, relative humidity, and wind fields, especially for daytime. A higher sensitivity to the physical parametrization was observed for nighttime.

Ethane is predominantly emitted from oil and NG production sites (Helmig et al., 2016; Xiao et al., 2008) and is a valuable chemical tracer to study the transport patterns of oil and NG emissions. To evaluate the impact of vertical mixing intensity on the distribution of pollutants, we compared the vertical distribution of ethane concentrations between the simulations. Figure 3 shows the diurnal cycle of averaged vertical cross section of ethane concentrations at PAO with measured PBL height for each simulation.

Complex local topography can cause localized transport patterns in the domain, which cannot be resolved at the model's 4 km x 4 km horizontal resolution. Pfister et al. (2017) discuss the impacts of the complicated wind patterns in the NFR and the limitations of WRF-Chem simulations in capturing the transport during FRAPPÉ campaign in details. To reduce the impact of localized influences on the sensitivity analysis we use airborne measurements which better represent the regional picture. Evaluation of modeled ethane concentrations with aircraft data provides information on the impact of different configurations on the transport of oil and NG emissions. Whisker plots of ethane concentrations at different elevations along the C130 morning and afternoon flights are shown in Figure 4. This plot limits the C130 observation to the NFR region (east of -105.2 longitude) to reduce transport errors, and it separates observations collected during 9:00 to noon (AM flights) and noon to 18:00 (PM flights) to account for the diurnal changes in PBLH. For this comparison, hourly model output has been interpolated to the time and location of each 1-minute average observation. Lower concentrations of ethane were measured during the PM flights compared to AM flights because of the higher PBLH and stronger vertical mixing in the afternoon (Figure 3). Table 5 summarizes the mean and NMB of ethane concentration for all simulations using ethane airborne measurements. In all simulations, the ethane concentrations are under-predicted by up to 3.3 ppb (NMB ranges between -63% to -42%) for the C130 AM flights and up to 1.7 ppb (NMB ranges between -47.6% to -29.5%) for the C130 PM flights. Overall, measured ethane concentrations, absolute biases, and absolute NMBs are higher for C130 AM compared to C130 PM. However, the differences between variability in NMBs for C130 AM and C130 PM are small i.e., 21% and 18.1%.

Measurements from P3 spirals focus on smaller regions and can capture the impact of local emissions. Figure 5 compares the vertical distribution of measured ethane concentrations against the corresponding model values (interpolated to time and location of each 1-min average observation) for all the simulations at BAO and Platteville (PAO) spirals. Both sites are located close to oil and NG sources (Figure 1), however urban emissions from Denver region can reach BAO (Pfister et al., 2017a). Similar to C130 observations, we illustrate the morning and afternoon data separately. Mean concentrations of up to 18.6 ppb (SD 2.8 ppb) were measured by P3 aircraft, but these high values were not captured by the model and resulted in biases up to -14.9 ppb (NMB of -80.5%) at PAO spirals and biases up to -7.16 ppb (NMB of -57.8%) at BAO spirals. Similar to C130 flights, higher measured ethane concentrations, absolute biases, and NMBs are observed for P3 AM flights compared to PM flights. Higher absolute biases and larger variance at lower altitude in AM flights and can be due to larger uncertainties in

capturing morning evolution of PBL. Variability in NMBs across simulations are greater in the PM spirals (42.8% at PAO and 57.3% at BAO) compared to AM spirals (36.5% at PAO and 31.3% at BAO).

While the model shows difficulty in representing the absolute magnitude in ethane concentrations in all simulations at lower altitudes, most simulations capture the changes in variance of ethane concentrations from lower to higher altitudes well especially for the C130 and P3 BAO flights. The C130 flights covered a larger region with varying flight patterns across the NFR, thus less variability in the modeled ethane concentrations was observed compared to the P3, which flew a repetitive pattern and the repeated spirals over the key surface locations reflect a higher influence from localized emissions.

3.2. Sensitivity to Planetary Boundary Layer Parametrization

We evaluated the sensitivity of WRF-Chem meteorological fields and ethane concentrations to a non-local (YSU) and two local (MYJ and MYNN3) PBL schemes in PBL1, PBL2, and PBL3 simulation, respectively. Table 2 includes details on simulation configurations. Temperature at BAO changed little between the different PBL schemes and the model agrees with observations (Figure 2). At all three altitudes, PBL1 had a small positive bias (errors less than 1°C) while PBL2 and PBL3 had a small negative bias (errors less than 1°C) (Table 3 and Table SM 2). Relative humidity differed slightly between local and non-local PBL parametrizations. PBL1 captured relative humidity well, especially at lower altitudes (mean bias of 0.38%, 1.47%, and 4.93% for 10m, 100m, and 300m respectively). PBL2 and PBL3 both over-predicted relative humidity at all altitudes. The mean bias for PBL2 and PBL3 ranged between 11.12% to 14.78% and 6.61% to 9.55%, respectively.

At all altitudes of BAO, PBL1 predicted higher wind speeds than observed as well as PBL2 and PBL3 (Figure 2, Figure SM 1-3). Wind direction does not vary significantly between PBL1, PBL2, and PBL3 at BAO tower and the model missed the southerly component of afternoon winds. Figure SM 4 shows the 10m average wind speed (during 1-August to 11-August) in PBL1, PBL2, and PBL3 for daytime and nighttime and compares it with measurements. Higher daytime wind speed was predicted by PBL1 in the Colorado Eastern plains, especially north of Denver and close to oil and NG operations. Figure SM 5 shows the averaged diurnal cycle of wind speed and wind direction at WC Tower and PAO (sites close to oil and NG operation). At WC tower and PAO, PBL2 and PBL3 better captured the southerly component of afternoon winds compared to BAO.

Each PBL scheme in the WRF model uses different diagnostics to determine the PBLH. To have a consistent comparison of PBL height in the three simulations, we used the 1.5-theta-increase method to estimate PBL height. In this method, PBLH is the lowest altitude where the difference between minimum potential temperature and potential temperature is greater than 1.5 K (Hu et al., 2010; Nielsen-Gammon et al., 2008). Figure 6 shows the diurnal evolution of PBLH as calculated using the 1.5-theta-increase method in the simulations. Observed PBLH at the PAO, Fort Collins (FC), and Golden-NREL sites were retrieved from micro-pulse Lidar backscatter profiles using Covariance Wavelet Transform (CWT) (Compton et al., 2013).

PBLH in the PBL1 simulation is greater than either PBL2, PBL3, or observations, and the bias is largest in the afternoon. Figure 3 (a, b, and c) shows PBL1 distributed ethane higher into the atmosphere and more dilution resulted in lower ethane concentration within the PBL. Figure SM 6 shows, on average, up to 5 ppb higher surface ethane concentrations in simulations based on local PBL schemes (PBL2 and PBL3) compared to the simulation based on non-local PBL scheme (PBL1).

The high bias in temperature, wind speed, and PBLH in PBL1, non-local PBL scheme, suggests a strong vertical mixing that is more defined in the Colorado Eastern plains and close to the oil and NG activities. The local PBL schemes (i.e. PBL2 and PBL3) predict cooler and moister climates and lower PBLH, which indicates less vertical mixing. This is consistent with previous works that compared local and non-local PBL schemes in the WRF model (Angevine et al., 2012; Hu et al., 2010).

The comparison between C130 airborne measurements and modeled ethane concentrations across the NFR, as illustrated in Figure 4, shows biases between -2.5 ppb and -2.3 ppb for AM flights and between -1.7 ppb and -1 ppb for PM flights. Lower NMB variability (4%) was observed in the C130 AM with NMB ranging from -43.1% to -47.1% compared to C130 PM with NMB variability of 18% and NMB ranging from -29.5% to -47.6%. Similar to the C-130 comparison, Figure 5, the simulations

15 did not capture the high ethane values measured during P3-BAO and P3-PAO spirals. The sensitivity of modeled ethane profiles to the PBL scheme is larger in P3 flights compared to C130 flights, with NMB variability of 14.1% ranging from -58% to -44% for PAO AM flights and NMB variability of 32.4% ranging from -37.3% to -69.7% for the PAO PM flight. On average PBL1 predicted higher ethane concentrations during AM flights at lower altitudes compared to PBL2 and PBL3 (Figure 3). Faster evolution of morning PBL and stronger vertical mixing in PBL1 lofted pollutants (including ethane) higher

20 into the atmosphere in the morning (Figure 6). The rapid growth of morning PBL in PBL1 resulted in higher concentration of ethane at higher altitudes (0.5 to 2 km) compared to PBL2 and PBL3.

3.3. Sensitivity to re-initialization

We investigated the impact of daily initialization of meteorological fields on the model performance in capturing the transport

25 of pollutants. For this, we conducted a sensitivity simulation (Init5) in which each daily cycle started at 18 UTC from ERA-interim meteorological fields and ran for 30 hours. In the comparison free-running simulation, Init4, we initialized the model at the first time step using the ERA-interim model and ran the simulation from 24 July 2014 to 18 August 2014 freely. Physical configurations and meteorological and chemical initial and boundary conditions kept the same for these two simulations (Table 2). Figure 2 shows an up to 3°C bias in nighttime temperature in Init5, but good agreement with the measured temperature

30 during the day. Init4 showed better skill in capturing nighttime temperature compared to Init5, but predicted the lowest daytime temperature among all the simulations with a bias up to -3°C. On average, the NMB of the temperature at BAO100m is between 8.6% in Init5 and -6.0% in Init4 (Table 3), which is the largest variability in NMB temperature across the simulations. Similar to the temperature, relative humidity showed a strong sensitivity to re-initialization. Init4 predicted the highest relative humidity, with NMB of 39.2% and Init5 predicted the lowest relative humidity, with an NMB of -26.5% among the simulations

at BAO 100m (Table 3). Nighttime wind direction at BAO (Figure 2), PAO, and WC tower (Figure SM 2) had a strong southerly component in Init4 compared to Init5 and observations. In addition, Init4 predicted higher wind speeds compared to BAO measurements (Figure 2) and Init5. Figure 7 shows on average higher wind speed at 10m altitude across the domain in Init4 compared to Init5 and measurements at both daytime and nighttime.

When compared to C130-AM ethane concentrations (Figure 4), Init4 predicted the lowest ethane concentrations (a bias of -3.3 ppb and NMB of -63%) among all the simulations. This is likely due to the high bias in of wind speed in this simulation which resulted in lower concentrations of ethane (Figure 7). The ethane bias is ~-2.5 ppb and NMB is -47.9% in Init5 during C130-AM. Concentrations during the C130-PM flights showed a weak sensitivity to re-initialization with NMB ranging from -37.8% (Init4) to -40.1% (Init5). For the P3-BAO and P3-PAO spirals in both AM and PM flights, Init4 had the lowest ethane values compared to all the other simulations and compared to observations (Figure 5). This resulted in the largest NMB variability across the simulations. During PAO AM, NMB ranges between -80.5% for Init4 and -53.2% for Init5 (NMB variability of 27.3%) and during PAO PM, NMB ranges between -72.9% for Init4 and -30.0% for Init5 (NMB variability of 43.9%).

3.4.   Sensitivity to meteorological initial and boundary condition

We tested the performance of changing the meteorological initial and boundary conditions by comparing simulations using ERA-Interim (Met5) with simulations using NCEP-FNL (Met6). As was done for Met5, we initialized meteorological fields with the re-analysis fields every day allowing for a 6-hour spin-up. To prepare meteorological initial and boundary conditions from global models, WRF interpolates these outputs to the designed domains. Figure SM 7 illustrates the differences between ERA-interim and NCEP-FNL model outputs interpolated to the outer domain at the lowest model level and averaged during August 1 to 15, 2014. Overall, the wind speed predictions by these two global models are very similar with slightly (less than 1 m/s) higher prediction by NCEP-FNL. ERA-interim and NCEP-FNL had larger discrepancies in temperature and relative humidity throughout the domain. Comparison with BAO observations (not shown) indicates similar performance for both models with somewhat lower temperature and higher relative humidity in ERA-interim compared to NCEP-FNL. These discrepancies did not have a large impact on temperature and relative humidity in the WRF-Chem simulation, however. Figure 2 and Figure SM 1-3 indicate that the performance of the two simulations is comparable in capturing temperature and relative humidity with a better agreement with measurements during the day. Met5 had slightly higher temperature and lower relative humidity compared to Met6 and compared better to measurements especially during the night. This is because WRF-Chem only uses the global values as the initial and boundary values and resolves for atmospheric variables such as temperature and relative humidity in high resolution based on physical parametrizations set for the simulation.

Comparison of ethane measurements by the C-130 and P3 aircraft with Met5 and Met6, shown in Figure 4 and Figure 5, respectively, also reflects an overall low sensitivity of the model performance to meteorological initial and boundary condition

for both AM and PM flights. High sensitivity was observed during P3-PAO PM flight with ethane NMB variability of 23.9% where Met5 had a bias of -2.6 ppb (NMB of -30%) and Met6 had -4.7 ppb (NMB of -53.9%).

3.5. Sensitivity to Horizontal resolution

The two nested domains in simulation Hor5 had a horizontal resolution of 12 km × 12 km (coarse) and 4 km × 4 km (fine). The one-way nesting method was used to prevent any feedback from the higher resolution inner domain on the outer domain. This means that while the outer domain provides the lateral boundary conditions to the inner domain, the higher resolution fields from the inner domain do not alter the outer domain fields. To compare the impact of horizontal resolution, we compared the performance of the coarse domain with the fine domain in the same simulation (5Hor). Temperature and relative humidity did not show significant sensitivity to the horizontal resolution at BAO and PAO, as neither did surface winds at BAO (Figure 2), PAO, and WC tower (Figure SM 4). At 100m and 300m altitudes at BAO, the coarse domain predicted higher nighttime wind speed compared to the fine domain and the measurements.

Averaged ethane concentrations along the C130 flights (Figure 4) do not vary significantly with horizontal resolution. However, higher differences are observed for the P3 spirals. This might be due to the C130 flights covering a larger area and, in parts, averaging out the impact of horizontal resolution, whereas the P3 spirals capture small-scale transport patterns in the domain more effectively. For the P3 spirals (Figure 5), the ethane NMB during BAO PM is +11.6% for the fine domain and -21.6% for the coarse domain. These values are -30% and -55.1% during PAO PM flights, respectively.

3.6. Oil and NG emission in the NFR

We assessed the performance of the model in capturing oil and NG emissions by focusing on ethane, which is mostly emitted from oil and NG emission sources, and on species with multiple emission sources such as CO and other VOCs. To investigate the contribution of oil and NG emissions to NFR air quality, we ran two additional simulations: in the one, the emissions are based on the NEI-2011 as provided (base simulation or Em7), in the other we doubled the oil and NG emissions (perturbed simulation or Em8).

Figure 8 shows the C130 PM measurements and bias limited to altitudes below 2000m and Figure 9 displays scatterplots of measured to modeled species concentrations limited to NFR, below 2000m with measured ethane greater than 2ppb. Figure 8a and b illustrate high values of ethane concentrations in the vicinity of oil and NG facilities which were not captured by the model resulting in low biases. As can be expected, the simulated ethane concentrations show a high sensitivity to changes in the oil and NG emissions (Figure SM 8). The highest sensitivity was observed for measurements taken over regions close to oil and NG sources, such as the P3-PAO spirals. Ethane biases between Em7 and Em8 varied from -9.4 ppb to -1 ppb (NMB from -50.8% to -5.5%) during P3-PAO AM, and from -2.7 ppb to +2.8 ppb (-31.2% to +31.8%) during P3-PAO PM. Doubling

oil and NG emissions lowered the absolute bias during the AM flights (NMB from -50.8% to -5.5%), but resulted in an overestimation of ethane concentrations during the PM flights (NMB from -31.2% to +31.8%). One possible reason for the difference between AM and PM biases might be an incorrect representation of the diurnal variation of ethane emission rates in the NEI-2011. An inverse modeling technique, as will be subject of further studies, can be used to calculate optimal scaling factors for hourly ethane emissions with the goal to minimize the discrepancies between model and measurement.

CO is mostly emitted from combustion processes and is released from many different source sectors. Figure 8c shows CO enhancements over both Denver and oil and NG facilities. Biases along the C130 flight tracks (Figure 8d) show an over-prediction of CO over Denver and west of Denver and an under-prediction over the oil and NG facilities. The scatterplot in Figure 9b reflects an overall low bias in modeled CO can be partly due to errors in capturing background CO. Doubling oil and NG emissions in Em8 only marginally increased the slope of the regression line indicating a low sensitivity of CO in the NFR to oil and NG emissions. This suggests that the source of the low bias in CO likely is related to other source categories and/or the model lateral boundary conditions.

In the RACM chemical mechanism, alkanes such as propane, n-butane, isobutane, and acetylene (ethyne), and alcohols such as methanol and ethanol are lumped under the "HC3" group (Stockwell et al., 1990). We compared the simulated HC3 concentrations with the sum of measured chemicals in the HC3 group during C130 flights. Similar to ethane, the highest values of HC3 were measured over oil and NG facilities (Figure 8c). These enhancements were not captured in the model and resulted in low model biases (Figure 7f). Comparison of measured HC3 with modeled values from Em7 and Em8, Figure 9c, confirms the low bias of HC3 and shows some increase in the slope of the regression line in Em8 albeit less pronounced compared to ethane.

Toluene and benzene are lumped together in the RACM chemistry under "TOL" (Stockwell et al., 1990). We compared simulated TOL with the sum of toluene and benzene concentrations observed during the C130 flights. The transport sector is a strong source of toluene and benzene in the NFR as well as oil and NG activities. TOL enhancements were observed over oil and NG facilities and Denver with higher values associated with oil and NG emissions (Figure 8g). The model did not capture the enhancements in regions influenced by oil and NG emissions, but well captured TOL values over Denver (Figure 7h). TOL showed very low sensitivity to perturbed oil and NG emissions as shown in Figure 9d. TOL emissions from oil and NG sector in the emission inventory used in this study (NEI-2011) were very low thus doubling oil and NG emissions did not increase TOL in the Em8. Similar to toluene and benzene, xylene enhancements were measured over oil and NG facilities and Denver. Model underestimated xylene enhancements over oil and NG activities and overestimated these enhancements over Denver. Em8 with doubled oil and NG emissions showed very similar performance to Em7 which indicates low emission rates of xylene from oil and NG sector in the NEI-2011 (not shown).

Figure 10 illustrates the HC3 to TOL ratio measured along the C130 PM limited to NFR region and altitudes below 2000m and the corresponding model values. Figure 10a shows oil and NG influenced points with enhanced measured ethane (concentrations greater than 2 ppb). HC3 to TOL ratios in oil and NG influenced locations show inconsistency between measured (HC3/TOL = 68) and Em7 modeled ratios (HC3/TOL = 22) which was improved in the Em8 (HC3/TOL = 40.9). However, doubling oil and NG emission still resulted in underestimations of HC3, TOL, and their ratios in this region. Figure 10b shows urban influenced points with low measured ethane (concentrations less than 2 ppb). Modeled HC3 to TOL ratios (7.3 for Em7 and 8.9 for Em8) in the urban influenced locations did not show large sensitivity to oil and NG emissions and agreed well with the measurements (10.2). In both oil and NG and urban influenced regions models predicted lower than measured Y-intercepts which was not improved in Em8. Figure 9c also confirms the low bias (about -2ppb) in background HC3 in the model. One reason for this offset can be underestimation in HC3 concentration in the lateral boundary condition fields or leakage from the NG distribution system which was not captured in the model.

The results suggest that HC3, toluene, benzene, and xylene from oil and NG sector are significantly underestimated in the NEI-2011. The low model bias for these species is more pronounced compared to the low model bias in ethane (Figure 9). The inconsistency between these biases implies that the NEI-2011 emission ratios might need to be changed and HC3, toluene, benzene, and xylene oil and NG emissions would need to be increased by a larger factor than ethane.

4. Conclusion

We used WRF-Chem to understand the sensitivity of pollutant transport at a high horizontal resolution to different model configurations with the focus on oil and NG emissions. By conducting a range of different sensitivity simulations, we assessed the variability of meteorological variables such as temperature, relative humidity, and wind fields as well as of ethane concentrations (used as a tracer for the oil and NG sector) to different model configurations and parameterizations. The overall daily cycle of temperature and relative humidity was captured well in the simulations with NMB ranging from -3.9% to 11.1% in temperature and from 29.7% to 52.6% in relative humidity. All simulations showed good skill in capturing daytime wind fields but showed higher biases for nighttime wind speeds.

Table 5 summarizes the mean and NMB for ethane concentrations from C130 and P3 airborne measurements below 2000m agl and the corresponding model values for all sensitivity tests. Significant underestimation of ethane in all simulations– especially in regions close to oil and NG activities – with biases up to -14.9 ppb (NMB up to -80.5%) suggest that the emission inventory used (NEI-2011) under-predicts oil and NG emissions. NMB variability (Table 5) was used as a proxy for variability in the model performance caused by model configurations. NMB of the near-surface ethane concentration for aircraft flight patterns across sensitivity simulations varied by up to 57.3% for P3-BAO, by up to 42.8% for P3-PAO and by up to 21.1% for C130 flights. The lower NMB variability during C130 flight can be due to the larger area coverage by this aircraft during the FRAPPÉ campaign and the irregular flight patterns. P3 spirals, covering smaller regions within the domain during repetitive

flight patterns, focused more on the local emissions and smaller scale transport patterns and captured a larger ethane sensitivity to model configurations. The largest sensitivity occurred in the initialization test (comparing daily re-initialization with free-run simulation) with ethane NMB variability up to 57.3%, followed by the horizontal resolution test (comparing horizontal resolution of 12 km × 12 km with 4 km × 4 km) and the PBL parametrization test (comparing local with non-local PBL

5   schemes) with ethane NMB variability up to 33.3% and 32.4%, respectively. To further investigate the performance of the model in capturing oil and NG emissions in the NFR we used a similar domain set-up with 12 km × 12 km and 4 km × 4 km horizontal resolution for outer and inner domains, respectively, daily re-initialization of meteorological variables with ERA-interim model, and MYNN3 PBL scheme.

10   We compared measured ethane, CO, lumped alkanes (HC3), lumped toluene and benzene (TOL), and xylene to corresponding modeled values and assessed the changes in the model performance when doubling oil and NG emissions. The model showed under-prediction of ethane with the original inventory and a strong sensitivity of ethane concentrations to oil and NG emissions. Doubling oil and NG emissions resulted in an improvement during AM flights and an overestimation of ethane during the PM flights which suggests possible incorrect representation of the diurnal variation of ethane emission rates in the NEI-2011. The

15   model tends to overestimate CO over the Denver region and underestimates CO over the oil and NG region. Low sensitivity of CO to oil and NG emissions indicates that CO in the region is predominantly emitted from sources other than oil and NG. Enhancements of HC3, TOL, xylene over oil and NG facilities were not fully captured in the model and resulted in low biases. Doubling emissions from oil and NG emissions improved the model performance in capturing HC3, but still resulted in a low model bias. Although high values of TOL and xylene were measured over oil and NG facilities, the model did not capture

20   these enhancements in either the simulations with base NEI-2011 emissions or doubled oil and NG emissions. The inconsistency between the sensitivity of ethane, HC3, benzene, toluene, and xylene to the increase in oil and NG emissions and mismatch between VOC ratios in the model and measurement suggest that oil and NG emission rates in the NEI-2011 need to be scaled differently for these species. VOC ratios in the measurements can be used to update these ratios in the emissions inventory.

We recognize that using ethane as a tracer to assess the sensitivity of WRF-Chem model to physical can be limited by the biases in the emission inventory. Conducting WRF-Chem simulations using different physical parametrization and using NMB variability can help to reduce this limitation. The presented results reflect the challenges that one is faced with when attempting to improve emission inventories by contrasting measured with modeled concentrations, either through simple direct

30   comparisons or more advanced methods, such as inverse modeling. Any uncertainties that arise from the model configuration will translate into the derived emission constraints, and it is important to be aware of the uncertainties resulting from different model setups. The WRF-Chem simulations and knowledge gained from this study will be used to support inverse modeling studies aimed to improve estimates of emission from oil and NG sector in the NFR.

Acknowledgements

The authors would like to acknowledge the FRAPPÉ and DISCOVER-AQ science team. The authors acknowledge the use of
WRF-Chem version 3.6.1 and the NCAR Command Language (UCAR/NCAR/CISL/TDD, 2017). We acknowledge Stuart
McKeen (NOAA) for providing NEI-2011 emission inventory, Bradley Pierce (NOAA) for providing RAQMS model outputs
for chemical initial and boundary conditions, and Ravan Ahmadov (NOAA) for help with conducting WRF-Chem simulations.
We thank Gordon Pierce (CDPHE/APCD) and Erick Mattson (CDPHE/APCD) for providing wind data at CDPHE site, Daniel
Wolfe (NOAA) for providing meteorological data at BAO tower, William Brune (Pennsylvania State University) for providing
meteorological data at PAO site. We further acknowledge Teresa Campos (NCAR/ACOM) for C130 CO measurements, Lisa
Kaser (NCAR) for C130 PTR-MS VOC measurements, Eric Apel (NCAR/ACOM) for C130 TOGA VOC measurements, Don
Blake (UC Irvine) for aircraft VOC WAS measurements. The University of Iowa group activities are partly funded by Regional
Scale Modeling in Support of KORUS-AQ: Improving Predictions of Dynamic Air Quality using Aircraft, Ground Networks,
and Satellite Data (Award No: NNX15AU17G) and Regional-Scale Analysis of Gas and Aerosol Distributions and the
Development of Emissions in Support of the NASA SEAC4RS Mission (Award No: NNX12AB78G). This work was
supported by computational resources provided by the University of Iowa.

Reference:

Ahmadov, R., McKeen, S., Trainer, M., Banta, R., Brewer, A., Brown, S., Edwards, P. M., De Gouw, J. A., Frost, G. J., Gilman, J., Helmig, D., Johnson, B., Karion, A., Koss, A., Langford, A., Lerner, B., Olson, J., Oltmans, S., Peischl, J., Pétron, G., Pichugina, Y., Roberts, J. M., Ryerson, T., Schnell, R., Senff, C., Sweeney, C., Thompson, C., Veres, P. R., Warneke, C., Wild, R., Williams, E. J., Yuan, B. and Zamora, R.: Understanding high wintertime ozone pollution events in an oil- and natural gas-producing region of the western US, Atmos. Chem. Phys., 15(1), 411–429, doi:10.5194/acp-15-411-2015, 2015.

Allen, D. T.: Emissions from oil and gas operations in the United States and their air quality implications, J. Air Waste Manage. Assoc., 66(6), 549–575, doi:10.1080/10962247.2016.1171263, 2016.

Alvarez, R. A., Pacala, S. W., Winebrake, J. J., Chameides, W. L. and Hamburg, S. P.: Greater focus needed on methane leakage from natural gas infrastructure., Proc. Natl. Acad. Sci. U. S. A., 109(17), 6435–40, doi:10.1073/pnas.1202407109, 2012.

Angevine, W. M., Eddington, L., Durkee, K., Fairall, C., Bianco, L. and Brioude, J.: Meteorological model evaluation for CalNex 2010, Mon. Weather Rev., 3885–3906, doi:10.1175/MWR-D-12-00042.1, 2012.

Arakawa, A., Jung, J. H. and Wu, C. M.: Toward unification of the multiscale modeling of the atmosphere, Atmos. Chem. Phys., 11(8), 3731–3742, doi:10.5194/acp-11-3731-2011, 2011.

Barkley, Z. R., Lauvaux, T., Davis, K. J., Deng, A., Miles, N. L., Richardson, S. J., Cao, Y., Sweeney, C., Karion, A., Smith, M., Kort, E. A., Schwietzke, S., Murphy, T., Cervone, G., Martins, D. and Maasakkers, J. D.: Quantifying methane emissions from natural gas production in north-eastern Pennsylvania, Atmos. Chem. Phys, 17, 13941–13966, doi:10.5194/acp-17-13941-2017, 2017.

Brandt, A. R., Heath, G. A., Kort, E. A., O'Sullivan, F., Petron, G., Jordaan, S. M., Tans, P., Wilcox, J., Gopstein, a M., Arent, D., Wofsy, S., Brown, N. J., Bradley, R., Stucky, G. D., Eardley, D. and Harriss, R.: Methane Leaks from North American Natural Gas Systems, Science (80-.)., 343(6172), 733–735, doi:10.1126/science.1247045, 2014.

Cheadle, L. C., Oltmans, S. J., Pétron, G., Schnell, R. C., Mattson, E. J., Herndon, S. C., Thompson, A. M., Blake, D. R. and Mcclure-begley, A.: Surface ozone in the Northern Front Range and the influence of oil and gas development on ozone production during FRAPPE / DISCOVER-AQ, Elem. Sci. Anthr., 6, doi:http://doi.org/10.1525/elementa.254, 2017.

Chou, M.-D. and Suarez, M. J.: Technical Report Series on Global Modeling and Data Assimilation A Thermal Infrared Radiation Parameterization for Atmospheric Studies Revised May 2003 i, Nasa Tech. Memo., 15(104606), 40, 1999.

Colorado Oil and Gas Conservation Commission: COGIS - Production Data Inquiry, [online] Available from: http://cogcc.state.co.us/data.html#/cogis (Accessed 1 January 2017), 2017.

Compton, J. C., Delgado, R., Berkoff, T. A. and Hoff, R. M.: Determination of planetary boundary layer height on short spatial and temporal scales: A demonstration of the covariance wavelet transform in ground-based wind profiler and lidar

measurements, J. Atmos. Ocean. Technol., 30(7), 1566–1575, doi:10.1175/JTECH-D-12-00116.1, 2013.

Conley, S., Franco, G., Faloona, I., Blake, D. R., Peischl, J. and Ryerson, T. B.: Methane emissions from the 2015 Aliso Canyon blowout in Los Angeles, CA, Science (80-.)., 2348(October 2015), 2–7, doi:10.1126/science.aaf2348, 2016.

Cuchiara, G. C., Li, X., Carvalho, J. and Rappenglück, B.: Intercomparison of planetary boundary layer parameterization and
5 its impacts on surface ozone concentration in the WRF/Chem model for a case study in Houston/Texas, Atmos. Environ., 96, 175–185, doi:dx.doi.org/10.1016/j.atmosenv.2014.07.013, 2014.

Cui, Y. Y., Brioude, J., Frost, G. J., Peischl, J., Ryerson, T., Trainer, M., Wofsy, S. C., Santoni, G. W. and Kort, E. a.: Top-Down Estimate of Methane Emissions in California Using a Mesoscale Inverse Modeling Technique, 13th Annu. C. Conf., 1–6, doi:10.1002/2014JD023002, 2014.

10 Cui, Y. Y., Brioude, J., McKeen, S. A., Angevine, W. M., Kim, S. W., Frost, G. J., Ahmadov, R., Peischl, J., Bousserez, N., Liu, Z., Ryerson, T. B., Wofsy, S. C., Santoni, G. W., Kort, E. A., Fischer, M. L. and Trainer, M.: Top-down estimate of methane emissions in California using a mesoscale inverse modeling technique: The San Joaquin Valley, J. Geophys. Res. Atmos., 122, 3686–3699, doi:10.1002/2014JD023002, 2017.

Dingle, J. H., Vu, K., Bahreini, R., Apel, E. C., Campos, T. L., Flocke, F., Fried, A., Herndon, S., Hills, A. J., Hornbrook, R.
15 S., Huey, G., Kaser, L., Montzka, D. D., Nowak, J. B., Reeves, M., Richter, D., Roscioli, J. R., Shertz, S., Stell, M., Tanner, D., Tyndall, G., Walega, J., Weibring, P. and Weinheimer, A.: Aerosol optical extinction during the front range air pollution and photochemistry Éxperiment (FRAPPÉ) 2014 summertime field campaign, Colorado, USA, Atmos. Chem. Phys., 16(17), 11207–11217, doi:10.5194/acp-16-11207-2016, 2016.

Energy information administration of US Department of Energy.: International energy outlook 2016-Natural gas, in
20 International energy outlook 2016, pp. 37–60., 2016.

European Centre for Medium-Range Weather Forecasts (ECMWF): ERA-Interim Project, , doi:10.5065/D6CR5RD9, 2009.

Fried, A.: Fast Airborne Spectroscopic Measurements of Formaldehyde and Ethane During the 2014 Front Range Air Pollution and Photochemistry Éxperiment (FRAPPÉ), Color. Dep. Public Heal. Environ., 1–6, 2015.

Gilman, J. B., Lerner, B. M., Kuster, W. C. and De Gouw, J. A.: Source signature of volatile organic compounds from oil and
25 natural gas operations in northeastern Colorado, Environ. Sci. Technol., 47(3), 1297–1305, doi:10.1021/es304119a, 2013.

Grell, G. A. and Freitas, S. R.: A scale and aerosol aware stochastic convective parameterization for weather and air quality modeling, Atmos. Chem. Phys. Discuss., 14(10), 5233–5250, doi:10.5194/acp-14-5233-2014, 2014.

Grell, G. A., Peckham, S. E., Schmitz, R., McKeen, S. A., Frost, G., Skamarock, W. C. and Eder, B.: Fully coupled "online" chemistry within the WRF model, Atmos. Environ., 39(37), 6957–6975, doi:10.1016/j.atmosenv.2005.04.027, 2005.

30 Guenther, A. B., Jiang, X., Heald, C. L., Sakulyanontvittaya, T., Duhl, T., Emmons, L. K. and Wang, X.: The model of emissions of gases and aerosols from nature version 2.1 (MEGAN2.1): An extended and updated framework for modeling biogenic emissions, Geosci. Model Dev., 5(6), 1471–1492, doi:10.5194/gmd-5-1471-2012, 2012.

Halliday, H., Thompson, A. M., Wisthaler, A., Blake, D. R., Hornbrook, R. S., Mikoviny, T., Muller, M., Eichler, P., Apel, E. C. and Hills, A. J.: Atmospheric benzene observations from oil and gas production in the Denver-Julesburg Basin in July and

August 2014, J. Geophys. Res. Atmos., 121(18), doi:10.1002/ 2016JD025327., 2016.

Helmig, D., Rossabi, S., Hueber, J., Tans, P., Montzka, S. A., Masarie, K., Thoning, K., Plass-Duelmer, C., Claude, A., Carpenter, L. J., Lewis, A. C., Punjabi, S., Reimann, S., Vollmer, M. K., Steinbrecher, R., Hannigan, J. W., Emmons, L. K., Mahieu, E., Franco, B., Smale, D. and Pozzer, A.: Reversal of global atmospheric ethane and propane trends largely due to US oil and natural gas production, Nat. Geosci., 9(July), 490–495, doi:10.1038/ngeo2721, 2016.

Hong, S.-Y., Noh, Y. and Dudhia, J.: A new vertical diffusion package with an explicit treatment of entrainment processes., Mon. Weather Rev., 134(9), 2318–2341, doi:10.1175/MWR3199.1, 2006.

Howarth, R. W., Santoro, R. and Ingraffea, A.: Methane and the greenhouse-gas footprint of natural gas from shale formations, Clim. Change, 106(4), 679–690, doi:10.1007/s10584-011-0061-5, 2011.

Hu, X. M., Nielsen-Gammon, J. W. and Zhang, F.: Evaluation of three planetary boundary layer schemes in the WRF model, J. Appl. Meteorol. Climatol., 49(9), 1831–1844, doi:10.1175/2010JAMC2432.1, 2010.

Iacono, M. J., Delamere, J. S., Mlawer, E. J., Shephard, M. W., Clough, S. A. and Collins, W. D.: Radiative forcing by long-lived greenhouse gases: Calculations with the AER radiative transfer models, J. Geophys. Res. Atmos., 113(13), 2–9, doi:10.1029/2008JD009944, 2008.

Inness, A., Baier, F., Benedetti, A., Bouarar, I., Chabrillat, S., Clark, H., Clerbaux, C., Coheur, P., Engelen, R. J., Errera, Q., Flemming, J., George, M., Granier, C., Hadji-Lazaro, J., Huijnen, V., Hurtmans, D., Jones, L., Kaiser, J. W., Kapsomenakis, J., Lefever, K., Leitão, J., Razinger, M., Richter, A., Schultz, M. G., Simmons, A. J., Suttie, M., Stein, O., Thépaut, J. N., Thouret, V., Vrekoussis, M. and Zerefos, C.: The MACC reanalysis: An 8 yr data set of atmospheric composition, Atmos. Chem. Phys., 13(8), 4073–4109, doi:10.5194/acp-13-4073-2013, 2013.

Janjic, Z.: Nonsingular Implementation of the Mellor-Yamada Level 2.5 Scheme in the NCEP Meso model, Natl. Centers Environ. Predict., 1–61, 2001.

Janjic, Z., Emanuel, K. and M., Z.-R.: Comments on "Development and Evaluation of a Convection Scheme for Use in Climate Models," J. Atmos. Sci., 57(21), 3686–3686, 2000.

Karion, A., Sweeney, C., Kort, E. A., Shepson, P. B., Brewer, A., Cambaliza, M., Conley, S. A., Davis, K., Deng, A., Hardesty, M., Herndon, S. C., Lauvaux, T., Lavoie, T., Lyon, D., Newberger, T., Pétron, G., Rella, C., Smith, M., Wolter, S., Yacovitch, T. I. and Tans, P.: Aircraft-Based Estimate of Total Methane Emissions from the Barnett Shale Region, Environ. Sci. Technol., 49(13), 8124–8131, doi:10.1021/acs.est.5b00217, 2015.

Kim, S. W., Heckel, A., Frost, G. J., Richter, A., Gleason, J., Burrows, J. P., McKeen, S., Hsie, E. Y., Granier, C. and Trainer, M.: NO2 columns in the western United States observed from space and simulated by a regional chemistry model and their implications for NOx emissions, J. Geophys. Res. Atmos., 114(11), 1–29, doi:10.1029/2008JD011343, 2009.

Levi, M.: Climate consequences of natural gas as a bridge fuel, Clim. Change, 118(3–4), 609–623, doi:10.1007/s10584-012-0658-3, 2013.

Lyon, D. R.: Methane Emissions from the Natural Gas Supply Chain, in Environmental and Health Issues in Unconventional Oil and Gas Development, pp. 33–48, Elsevier Inc., 2015.

McDuffie, E. E., Edwards, P. M., Gilman, J. B., Lerner, B. M., Dube, W. P., Trainer, M., Wolfe, D. E., Angevine, W. M., DeGouw, J., Williams, E. J., Tevlin, A. G., Murphy, J. G., Fischer, E. V., McKeen, S., Ryerson, T. B., Peischl, J., Holloway, J. S., Aikin, K., Langfor, A. O., Sneff, C. J., Alvarez II, R. J., Hall, S. R., Ullmann, K., Lantz, K. O. and Brown, S. S.: Influence of oil and gas emissions on summertime ozone in the Colorado Northen Front Range, J. Geophys. Res., 1–19, doi:doi:10.1002/2016JD025265., 2016.

McJeon, H., Edmonds, J., Bauer, N., Clarke, L., Fisher, B., Flannery, B. P., Hilaire, J., Krey, V., Marangoni, G., Mi, R., Riahi, K., Rogner, H. and Tavoni, M.: Limited impact on decadal-scale climate change from increased use of natural gas, Nature, 514(7523), 482–485, doi:10.1038/nature13837, 2014.

McKenzie, L. M., Witter, R. Z., Newman, L. S. and Adgate, J. L.: Human health risk assessment of air emissions from development of unconventional natural gas resources, Sci. Total Environ., 424, 79–87, doi:10.1016/j.scitotenv.2012.02.018, 2012.

Nakanishi, M. and Niino, H.: Development of an Improved Turbulence Closure Model for the Atmospheric Boundary Layer, J. Meteorol. Soc. Japan, 87(5), 895–912, doi:10.2151/jmsj.87.895, 2009.

Natarajan, M., Pierce, R. B., Schaack, T. K., Lenzen, A. J., Al-Saadi, J. A., Soja, A. J., Charlock, T. P., Rose, F. G., Winker, D. M. and Worden, J. R.: Radiative forcing due to enhancements in tropospheric ozone and carbonaceous aerosols caused by Asian fires during spring 2008, J. Geophys. Res. Atmos., 117(6), 1–18, doi:10.1029/2011JD016584, 2012.

National Centers for Environmental Prediction, National Weather Service, NOAA, U. S. D. of C.: NCEP FNL Operational Model Global Tropospheric Analyses, continuing from July 1999, , doi:10.5065/D6M043C6, 2000.

Nielsen-Gammon, J. W., Powell, C. A., Mahoney, M. J., Angevine, W. M., Senff, C., White, A., Berkowitz, C., Doran, C. and Knupp, K.: Multisensor Estimation of Mixing Heights over a Coastal City, J. Appl. Meteorol. Climatol., 27–43, doi:10.1175/2007JAMC1503.1, 2008.

Olaguer, E. P.: The potential near-source ozone impacts of upstream oil and gas industry emissions, J. Air Waste Manag. Assoc., 62(8), 966–977, doi:10.1080/10962247.2012.688923, 2012.

Peischl, J., Karion, A., Sweeney, C., Kort, E. A., Smith, M. L., Brandt, A. R., Yeskoo, T., Aikin, K. C., Conley, S. A., Gvakharia, A., Trainer, M., Wolter, S. and Ryerson, T. B.: Quantifying atmospheric methane emissions from oil and natural gas production in the Bakken shale region of North Dakota, J. Geophys. Res. Atmos., 121, 6101–6111, doi:10.1002/2015JD024631, 2016.

Pétron, G., Frost, G., Miller, B. R., Hirsch, A. I., Montzka, S. A., Karion, A., Trainer, M., Sweeney, C., Andrews, A. E., Miller, L., Kofler, J., Bar-Ilan, A., Dlugokencky, E. J., Patrick, L., Moore, C. T., Ryerson, T. B., Siso, C., Kolodzey, W., Lang, P. M., Conway, T., Novelli, P., Masarie, K., Hall, B., Guenther, D., Kitzis, D., Miller, J., Welsh, D., Wolfe, D., Neff, W. and Tans, P.: Hydrocarbon emissions characterization in the Colorado Front Range: A pilot study, J. Geophys. Res. Atmos., 117(4), 1–19, doi:10.1029/2011JD016360, 2012.

Pétron, G., Karion, A., Sweeney, C., Miller, B. R., Montzka, S. A., Frost, G. J., Trainer, M., Tans, P., Andrews, A., Kofler, J., Helmig, D., Guenther, D., Dlugokencky, E., Lang, P., Newberger, T., Wolter, S., Hall, B., Novelli, P., Brewer, A., Conley, S.,

Hardesty, M., Banta, R., White, A., Noone, D., Wolfe, D. and Schnell, R.: A new look at methane and nonmethane hydrocarbon emissions from oil and natural gas operations in the Colorado Denver-Julesburg Basin, J. Geophys. Res. Atmos., 119(10), 5787–5805, doi:https://doi.org/10.1002/2013JD021272, 2014.

Pfister, G., Flocke, F., Hornbrook, R., Orlando, J. and Lee, S.: Process-Based and Regional Source Impact Analysis for FRAPPÉ and DISCOVER-AQ 2014. [online] Available from: https://www.colorado.gov/airquality/tech_doc_repository.aspx?action=open&file=FRAPPE-NCAR_Final_Report_July2017.pdf, 2017a.

Pfister, G. G., Reddy, P. J., Barth, M. C., Flocke, F. F., Fried, A., Herndon, S. C., Sive, B. C., Sullivan, J. T., Thompson, A. M., Yacovitch, T. I., Weinheimer, A. J. and Wisthaler, A.: Using Observations and Source-Specific Model Tracers to Characterize Pollutant Transport During FRAPPÉ and DISCOVER-AQ, J. Geophys. Res. Atmos., 122(19), 10510–10538, doi:10.1002/2017JD027257, 2017b.

Pierce, R. B., Schaack, T., Al-Saadi, J. A., Fairlie, T. D., Kittaka, C., Lingenfelser, G. S., Natarajan, M., Olson, J. R., Soja, A. J., Zapotocny, T., Lenzen, A., Stobie, J., Johnson, D., Avery, M. A., Sachse, G. W., Thompson, A., Cohen, R., Dibb, J. E., Crawford, J. H., Rault, D. F., Martin, R., Szykman, J. and Fishman, J.: Chemical data assimilation estimates of continental U.S. ozone and nitrogen budgets during the Intercontinental Chemical Transport Experiment-North America, J. Geophys. Res. Atmos., 112(12), doi:10.1029/2006JD007722, 2007.

Richter, D., Weibring, P., Walega, J. G., Fried, A., Spuler, S. M. and Taubman, M. S.: Compact highly sensitive multi-species airborne mid-IR spectrometer, Appl. Phys. B Lasers Opt., 119(1), 119–131, doi:10.1007/s00340-015-6038-8, 2015.

Saide, P. E., Carmichael, G. R., Spak, S. N., Gallardo, L., Osses, A. E., Mena-Carrasco, M. A. and Pagowski, M.: Forecasting urban PM10 and PM2.5 pollution episodes in very stable nocturnal conditions and complex terrain using WRF-Chem CO tracer model, Atmos. Environ., 45(16), 2769–2780, doi:10.1016/j.atmosenv.2011.02.001, 2011.

Skamarock, W. C., Klemp, J. B., Dudhia, J., O., G. D. and Barker, D. M.: A description of the Advanced Research WRF version 3. NCAR Tech. Note NCAR/TN-4751STR, 2008.

Smith, M. L., Kort, E. A., Karion, A., Sweeney, C., Herndon, S. C. and Yacovitch, T. I.: Airborne Ethane Observations in the Barnett Shale: Quantification of Ethane Flux and Attribution of Methane Emissions, Environ. Sci. Technol., 49(13), 8158–8166, doi:10.1021/acs.est.5b00219, 2015.

Sobhani, N., Kulkarni, S. and Carmichael, G. R.: Source Sector and Region Contributions to Black Carbon and PM2.5 in the Arctic, Atmos. Chem. Phys. Discuss., (in review), doi:10.5194/acp-2018-65, 2018.

Stockwell, W. R., Middleton, P., Chang, J. S. and Tang, X.: The second generation regional acid deposition model chemical mechanism for regional air quality modeling, J. Geophys. Res., 95(D10), 16343, doi:10.1029/JD095iD10p16343, 1990.

Stockwell, W. R., Kirchner, F., Kuhn, M. and Seefeld, S.: A new mechanism for regional atmospheric chemistry modeling, J. Geophys. Res., 102(D22), 25847, doi:10.1029/97JD00849, 1997.

Stull, R. B.: An introduction to boundary layer meteorology, Springer Science & Business Media., 1988.

Thompson, C. R., Hueber, J. and Helmig, D.: Influence of oil and gas emissions on ambient atmospheric non-methane

hydrocarbons in residential areas of Northeastern Colorado, Elem. Sci. Anthr., 2, 000035, doi:10.12952/journal.elementa.000035, 2014.

U.S. Energy Information Administration: International Energy Outlook 2016-Electricity, in International Energy Outlook, pp. 81–100. [online] Available from: http://www.eia.gov/forecasts/ieo/pdf/0484(2016).pdf, 2016.

5   U.S. Environmental Protection Agency: 2011 National Emissions Inventory, version 2 Technical Support Document. [online] Available from: https://www.epa.gov/sites/production/files/2015-10/documents/nei2011v2_tsd_14aug2015.pdf, 2015.

UCAR/NCAR/CISL/TDD: The NCAR Command Language (Version 6.4.0) [Software]., 2017.

Valerino, M. J., Johnson, J. J., Izumi, J., Orozco, D., Hoff, R. M., Delgado, R. and Hennigan, C. J.: Sources and composition of PM2.5 in the Colorado Front Range during the DISCOVER-AQ study, J. Geophys. Res. Atmos., 122(1), 566–582,

10   doi:10.1002/2016JD025830, 2017.

Vu, K. T., Dingle, J. H., Bahreini, R., Reddy, P. J., Campos, T. L., Diskin, G. S., Fried, A., Herndon, S. C., Hornbrook, R. S., Huey, G., Kaser, L., Montzka, D. D., Nowak, J. B., Richter, D., Roscioli, J. R., Shertz, S., Stell, M., Tanner, D., Tyndall, G., Walega, J., Weibring, P., Weinheimer, A. J., Pfister, G. and Flocke, F.: Impacts of the Denver Cyclone on Regional Air Quality and Aerosol Formation in the Colorado Front Range during FRAPPÉ 2014, Atmos. Chem. Phys. Discuss., (3), 1–40,

15   doi:10.5194/acp-2016-532, 2016.

Xiao, Y., Logan, J. A., Jacob, D. J., Hudman, R. C., Yantosca, R. and Blake, D. R.: Global budget of ethane and regional constraints on U.S. sources, J. Geophys. Res. Atmos., 113(21), 1–13, doi:10.1029/2007JD009415, 2008.

Yacovitch, T. I., Herndon, S. C., Roscioli, J. R., Floerchinger, C., McGovern, R. M., Agnese, M., Pétron, G., Kofler, J., Sweeney, C., Karion, A., Conley, S. A., Kort, E. A., Nähle, L., Fischer, M., Hildebrandt, L., Koeth, J., McManus, J. B., Nelson,

20   D. D., Zahniser, M. S. and Kolb, C. E.: Demonstration of an ethane spectrometer for methane source identification, Environ. Sci. Technol., 48(14), 8028–8034, doi:10.1021/es501475q, 2014.

Zavala-Araiza, D., Lyon, D. R., Alvarez, R. A., Davis, K. J., Harriss, R., Herndon, S. C., Karion, A., Kort, E. A., Lamb, B. K., Lan, X., Marchese, A. J., Pacala, S. W., Robinson, A. L., Shepson, P. B., Sweeney, C., Talbot, R., Townsend-Small, A., Yacovitch, T. I., Zimmerle, D. J. and Hamburg, S. P.: Reconciling divergent estimates of oil and gas methane emissions, Proc.

25   Natl. Acad. Sci., 112(51), 15597–15602, doi:10.1073/pnas.1522126112, 2015.

Table 1. Summary of basic WRF-Chem configuration

Category	Selected option
Horizontal resolution	12km and 4km
Vertical resolution	53 layers (11 within the lowest 1km)
Microphysics	Morrison double-moment scheme
Land Surface	5-layer thermal diffusion
Shortwave radiation	Goddard shortwave
longwave radiation	RRTMG scheme
Cumulus parametrization	Grell-Freitas scheme
Gas-phase chemistry	RACM-ESRL
Biogenic emission	MEGAN

Table 2. Summary of WRF-Chem configurations for sensitivity tests designed for this study. Sensitivity tests are divided by horizontal lines

Test	Sim. ID	Sim. Name	PBL Scheme	Met IC & BC	Chem IC & BC	Init.	Emiss.
PBL	PBL1	1-YFM	YSU (Y)	NCEP-FNL (F)	MACC (M)	Free run	NEI2011
	PBL2	2-MjFM	MYJ (Mj)	NCEP-FNL (F)	MACC (M)	Free run	NEI2011
	PBL3	3-MnFM	MYNN3 (Mn)	NCEP-FNL (F)	MACC (M)	Free run	NEI2011
Initialization	Init4	4-MnER	MYNN3 (Mn)	ERA-interim (E)	RAQMS (R)	Free run	NEI2011
	Init5	5-MnERi	MYNN3 (Mn)	ERA-interim (E)	RAQMS (R)	re-init (i)	NEI2011
Met IC & BC	Met5	5-MnERi	MYNN3 (Mn)	ERA-interim (E)	RAQMS (R)	re-init (i)	NEI2011
	Met6	6-MnFRi	MYNN3 (Mn)	NCEP-FNL (F)	RAQMS (R)	re-init (i)	NEI2011
Horizontal resolution	Hor5	5-MnERi	MYNN3 (Mn)	ERA-interim (E)	RAQMS (R)	re-init (i)	NEI2011
	Hor5-12km	5-MnERi-12km	MYNN3 (Mn)	ERA-interim (E)	RAQMS (R)	re-init (i)	NEI2011
Emission Inventory	Em7	5-MnERiMeg	MYNN3 (Mn)	ERA-interim (E)	RAQMS (R)	re-init (i)	NEI2011 + Megan
	Em8	7-MnERiMeg-2OnG	MYNN3 (Mn)	ERA-interim (E)	RAQMS (R)	re-init (i)	NEI2011 (doubled oil & NG) + Megan

Table 3. Summary of model performance in capturing temperature (T) and Relative Humidity (RH) at BAO 100m during 1 to 15 August 2014.

100m		PBL			Met IC and BC		Initialization		Horizontal resolution	
T(C)	OBS	PBL1	PBL2	PBL3	Met5	Met6	Init4	Init5	Hor5	Hor5-12km
Mean	22.01	22.18	21.15	21.52	23.92	23.20	20.70	23.92	23.92	23.90
R		0.85	0.83	0.81	0.81	0.84	0.63	0.81	0.81	0.82
RMSE		1.86	2.07	2.01	2.74	2.17	3.07	2.74	2.74	2.72
MAE		1.40	1.72	1.65	2.18	1.64	2.46	2.18	2.18	2.10
MB		0.17	-0.86	-0.5	1.90	1.19	-0.31	1.90	1.90	1.89
NMB(%)		0.8	-3.9	-2.3	8.6	5.4	-6.0	8.6	8.6	8.6
RH(%)	OBS	PBL1	PBL2	PBL3	Met5	Met6	Init4	Init5	Hor5	Hor5-12km
Mean	42.27	43.74	51.79	48.88	31.06	38.51	58.90	31.06	31.06	31.52
R		0.69	0.59	0.53	0.52	0.52	0.44	0.52	0.52	0.58
RMSE		11.90	16.33	14.67	16.69	13.63	25.90	16.69	16.69	16.00
MAE		9.21	13.47	12.31	12.79	10.28	21.17	12.79	12.79	11.99
MB		1.47	9.52	6.61	-11.21	-3.76	16.63	-11.21	-11.21	-10.75
NMB(%)		3.5	22.5	15.6	-26.5	-8.9	39.2	-26.5	-26.5	-25.4

Table 4. Summary of model performance in capturing wind speed and direction at BAO 100m during Aug 1-15, 2014

Day - 100 m		OBS	PBL			Met IC & BC		Initialization		Horizontal Res.	
			PBL1	PBL2	PBL3	Met5	Met6	Init4	Init5	Hor5	Hor5-12km
Wind Speed	Mean	3.22	3.84	3.40	2.70	2.87	3.19	3.77	2.87	2.87	2.76
	STD	2.02	2.14	2.26	1.57	1.57	1.80	2.86	1.57	1.57	1.45
Wind Direction	Mean	117.84	62.90	64.05	66.76	33.86	59.61	55.92	33.86	33.86	41.11
	STD	71.06	48.79	63.44	56.30	73.10	75.90	74.77	73.10	73.10	67.74
Night - 100 m		**OBS**	**PBL1**	**PBL2**	**PBL3**	**Met5**	**Met6**	**Init4**	**Init5**	**Hor5**	**Hor5-12km**
Wind Speed	Mean	3.42	4.69	4.06	3.57	4.02	4.41	4.87	4.02	4.02	4.73
	STD	1.81	2.34	2.78	2.47	2.45	2.32	2.88	2.45	2.45	3.15
Wind Direction	Mean	233.09	114.12	268.45	349.75	331.38	292.24	155.59	331.38	331.38	303.89
	STD	70.62	97.13	89.35	86.75	87.28	77.12	85.20	87.28	87.28	85.11

Table 5. Ethane mean, NMB, and NMB variability from C130 and P3 BAO and PAO airborne measurements below 2000m and the corresponding model values

			C130 - NFR		P3 - BAO		P3- PAO	
			AM	PM	AM	PM	AM	PM
	OBS	**Mean (ppb)**	5.22	3.49	12.39	4.90	18.56	8.66
PBL	**PBL1**	**Mean (ppb)**	2.97	1.83	8.51	3.85	7.79	2.62
		NMB (%)	-43.1	-47.6	-31.3	-21.4	-58.0	-69.7
	PBL2	**Mean (ppb)**	2.97	2.36	9.11	4.53	7.93	5.43
		NMB (%)	-43.1	-32.4	-26.5	-7.6	-57.3	-37.3
	PBL3	**Mean (ppb)**	2.76	2.46	8.67	4.90	10.40	4.20
		NMB (%)	-47.1	-29.5	-30	0	-44.0	-51.5
	All PBL	**NMB var. (%)**	4.0	18.1	4.8	21.4	14.1	32.4
Init.	**Init4**	**Mean (ppb)**	1.93	2.17	5.23	2.66	3.62	2.35
		NMB (%)	-63.0	-37.8	-57.8	-45.7	-80.5	-72.9
	Init5	**Mean (ppb)**	2.72	2.09	7.46	5.47	8.68	6.06
		NMB (%)	-47.9	-40.1	-39.7	11.6	-53.2	-30.0
	All Init	**NMB var. (%)**	15.1	2.3	18.0	57.3	27.3	42.8
Met IC & BC	**Met5**	**Mean (ppb)**	2.72	2.09	7.46	5.47	8.68	6.06
		NMB (%)	-47.9	-40.1	-39.7	11.6	-53.2	-30.0
	Met6	**Mean (ppb)**	3.03	1.92	7.00	4.46	7.90	3.99
		NMB (%)	-42.0	-45.0	-43.5	-9.0	-57.3	-53.9
	All Met	**NMB var. (%)**	5.9	4.9	3.7	20.6	4.2	23.9
Hor. Res	**Hor5**	**Mean (ppb)**	2.72	2.09	7.46	5.47	8.68	6.06
		NMB (%)	-47.9	-40.1	-39.7	11.6	-53.2	-30.0
	Hor5-12km	**Mean (ppb)**	2.60	1.98	5.67	3.84	5.68	3.89
		NMB (%)	-50.2	-43.3	-54.2	-21.6	-69.4	-55.1
	All res.	**NMB var. (%)**	2.3	3.2	14.4	33.3	16.2	25.1
Emiss	**Em7**	**Mean (ppb)**	2.76	2.16	7.59	5.26	9.13	5.96
		NMB (%)	-47.1	-38.1	-38.6	7.3	-50.8	-31.2
	Em8	**Mean (ppb)**	5.07	3.90	14.57	10.1	17.54	11.41
		NMB (%)	-2.9	11.7	17.6	106.1	-5.5	31.8
	All emiss	**NMB var. (%)**	44.3	49.9	56.3	98.9	45.3	62.9
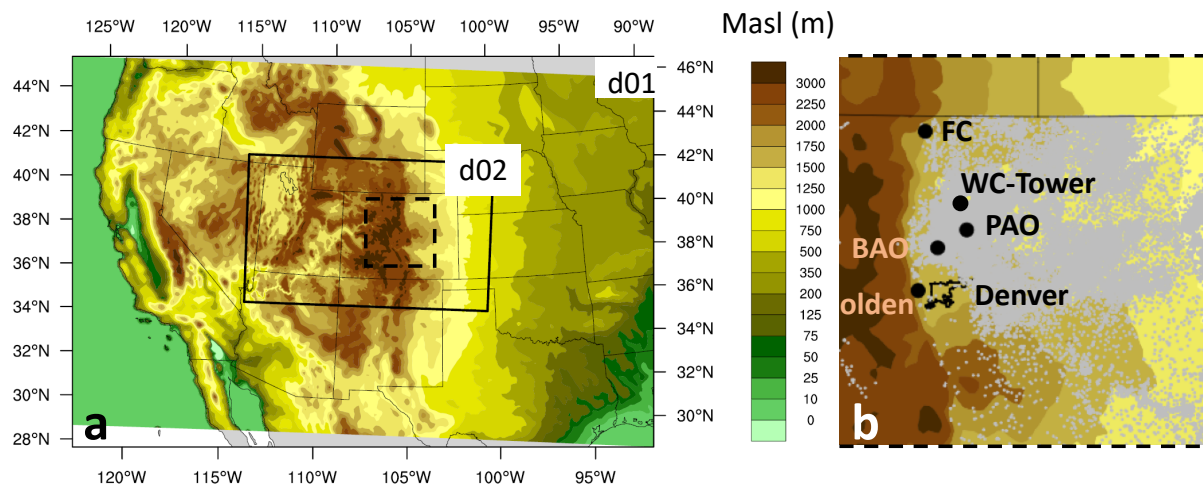
Figure 1. Terrain map of the WRF-Chem outer domain (d01) and inner domains (d02) and location of observation sites. a) shows the two nested domains designed for this study. b) shows the zoomed in map of domain 2 with the location of several sites. Grey dots show the location of permitted wells (http://cogcc.state.co.us/)
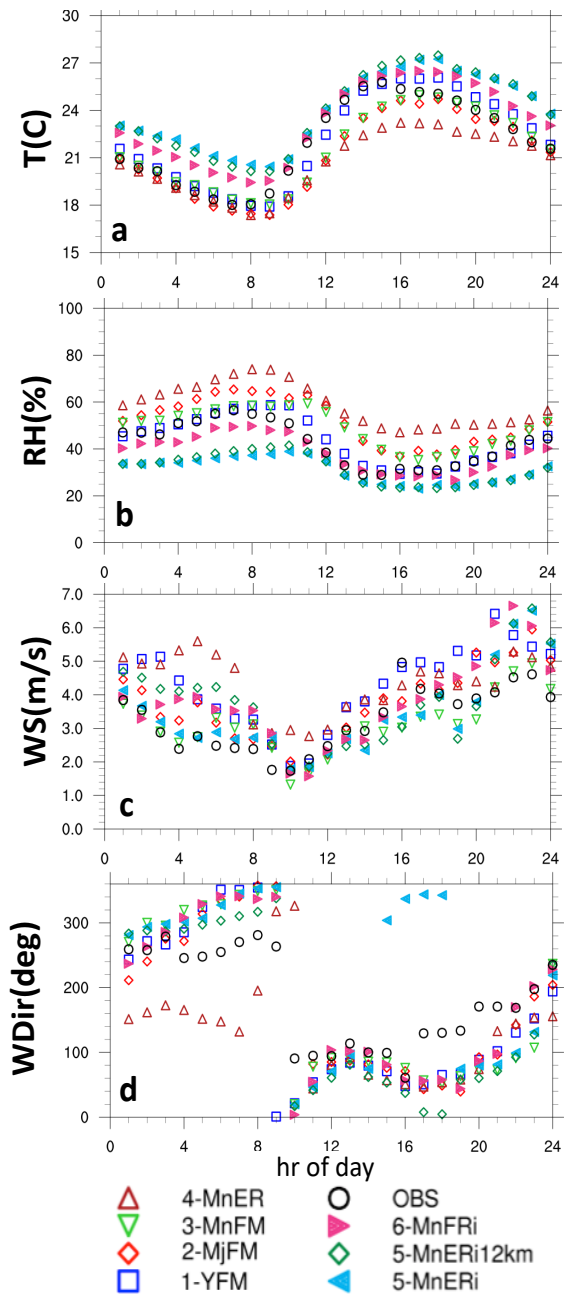
Figure 2. Average diurnal cycle of temperature (a), relative humidity (b), wind speed (c) and wind direction (d) for all tests and observation at BAO 100m. Averages are calculated for Aug 1 to 15, 2014.
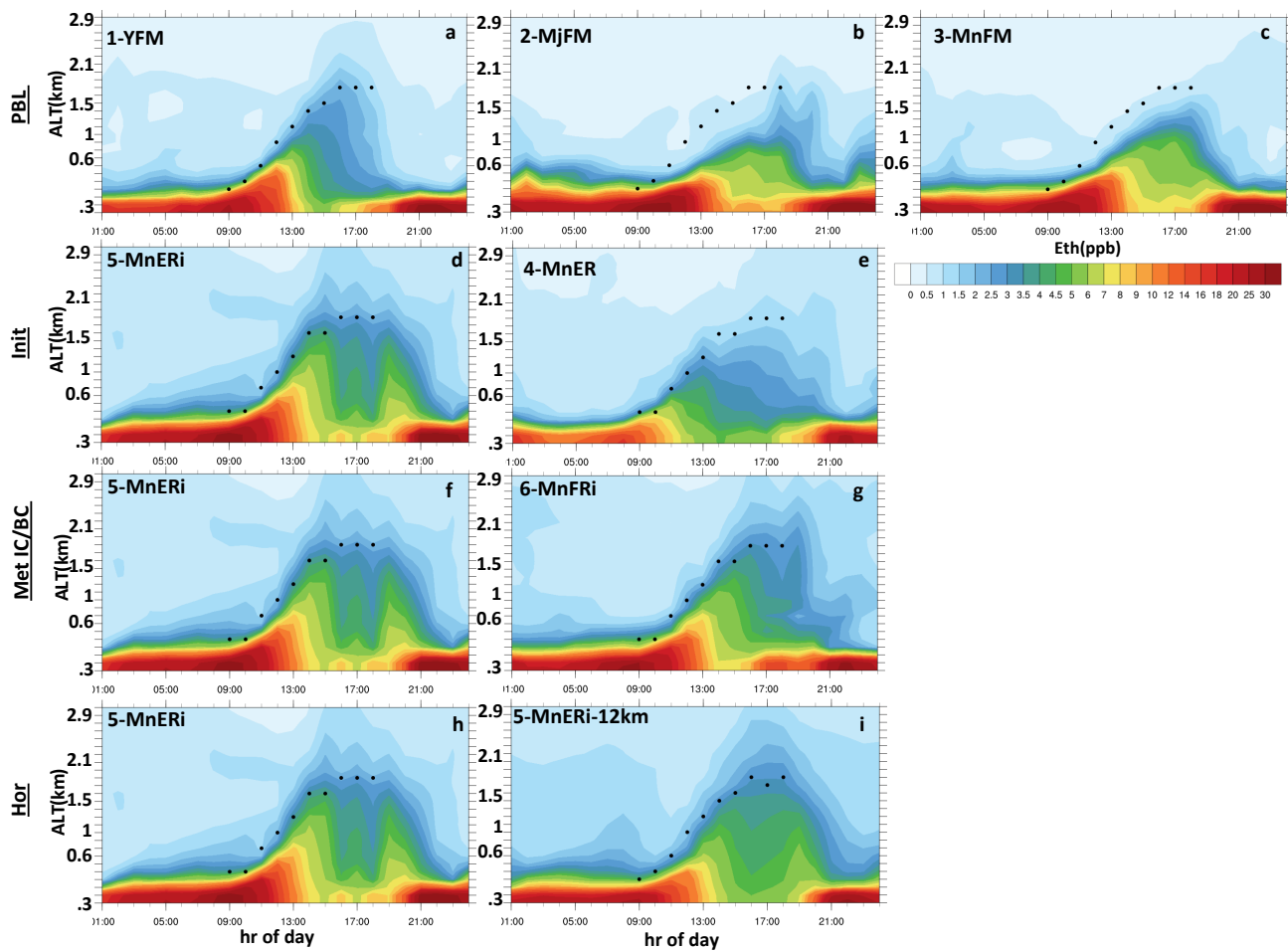
Figure 3 Cross section of modeled ethane at PAO and measured PBL height (black dots) averaged from August 1 to 10, 2014
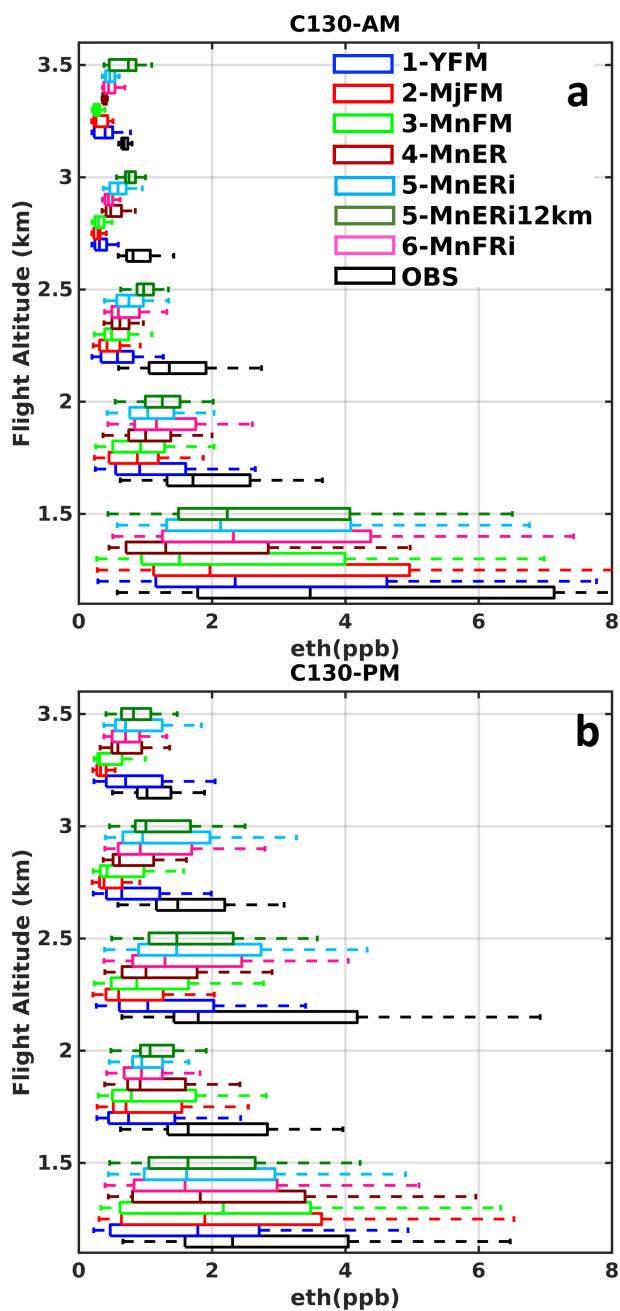
Figure 4. Vertical distribution of simulated and measured ethane in the NFR area separated by the flight time. (a) C130-AM 9am to noon observation and the corresponding model values. (b) C130-PM noon to 6pm observation and the corresponding model values. Measurement pointes were binned based on their elevation above the ground in 500m intervals. The first bin includes all measurements below 1.5km and the last bin includes all measurements above 3km
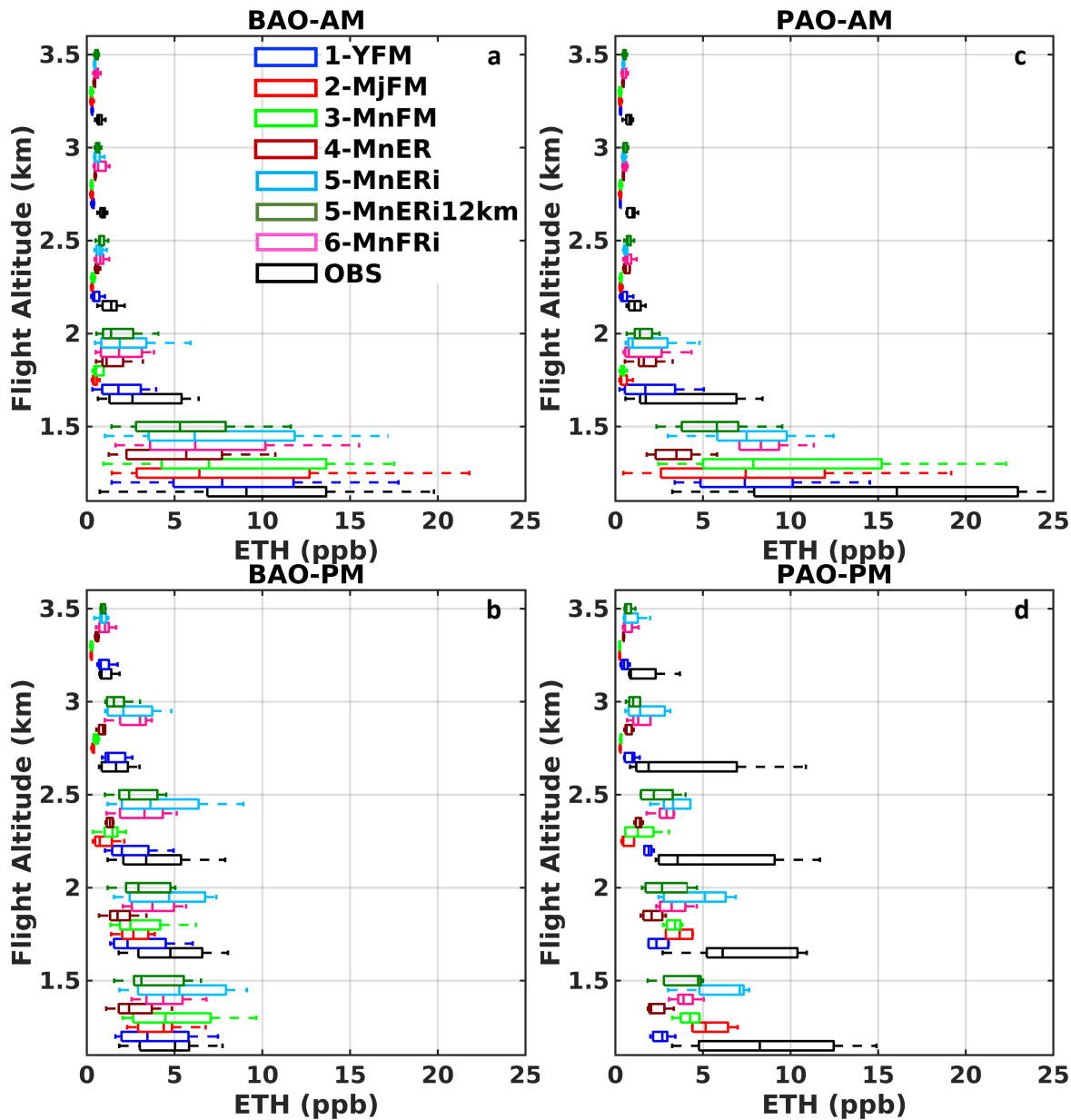
Figure 5. Vertical distribution of ethane at PAO (a and b) and BAO (c and d) site measured during P3 spiral flights and the corresponding model values. Flights are separated by the flight time. a and c show P3-AM that include 9am to noon observation and the corresponding model values. b and d show P3-PM that include noon to 6pm observation and the corresponding model values. Measurement pointes were binned based on their elevation above the ground in 500m intervals. The first bin includes all measurements below 1.5km and the last bin includes all measurements above 3km
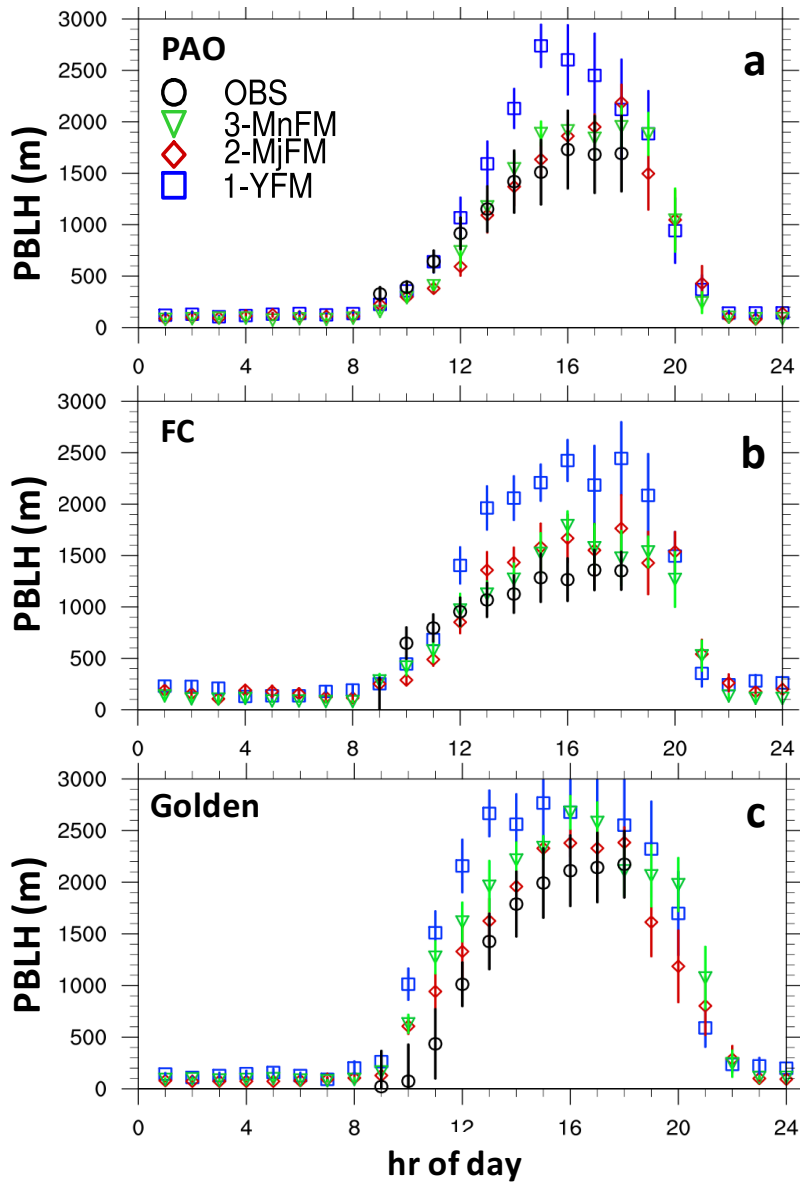
Figure 6. Diurnal evolution of PBL in MYJ, MYNN3, and YSU schemes at PAO (a), Fort Collins (b), and Golden-NREL (c) sites. PBLH was measured using micro-pulse Lidar backscatter profiles during the daytime. Error bars represent the standard error.
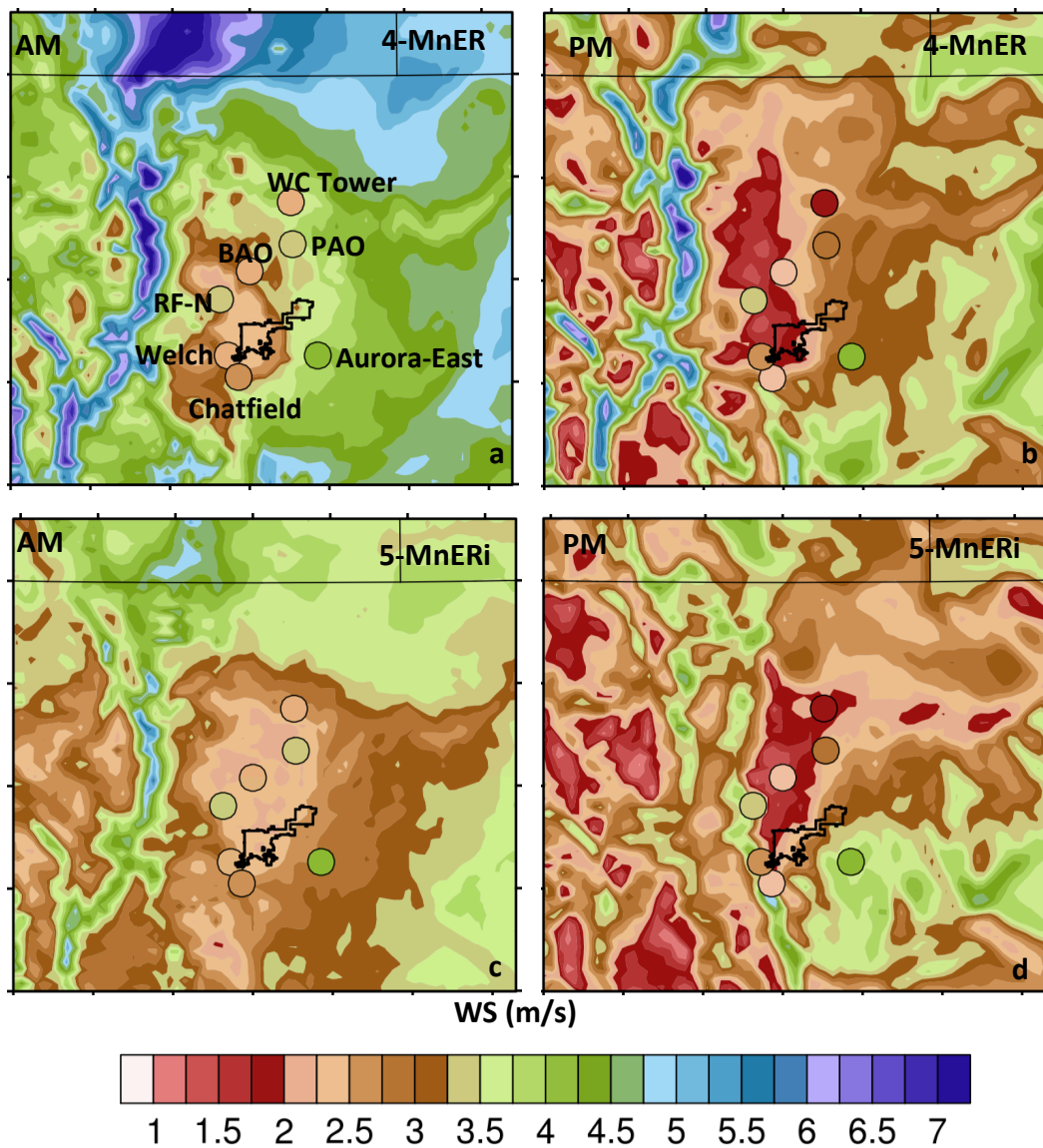
Figure 7 Measured (circles) and modeled (color contour) wind speed at 10m captured by Init4 (a and b) and Init5 (c and d) from Aug 1 to 11, 2014 and separated by daytime vs nighttime.
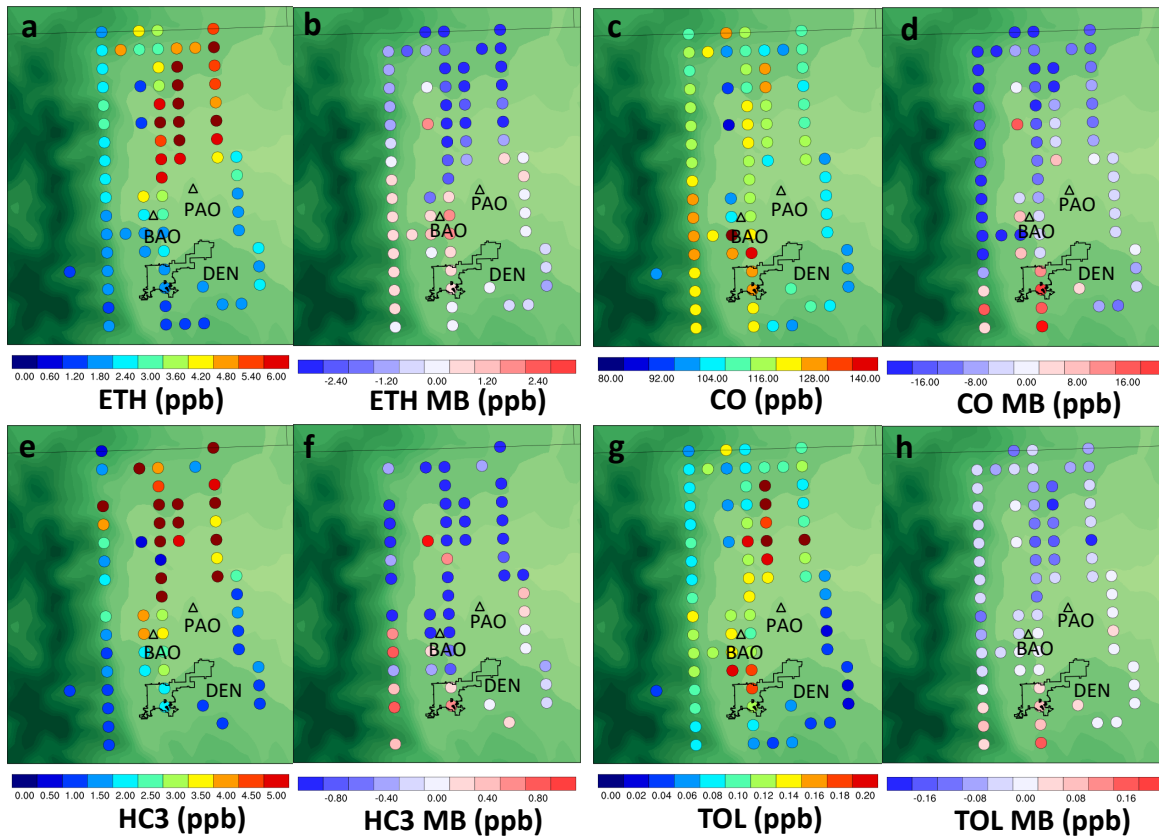
Figure 8. Mean and mean bias ethane concentration (a and b), CO (c and d), HC3 (e and f), and TOL (g and h) along the C130 PM flights are limited to measurements below 2000m agl and grids with more than 4 measurement points. The outline of Denver county and the locations of BAO and PAO are marked on the underlying terrain map.
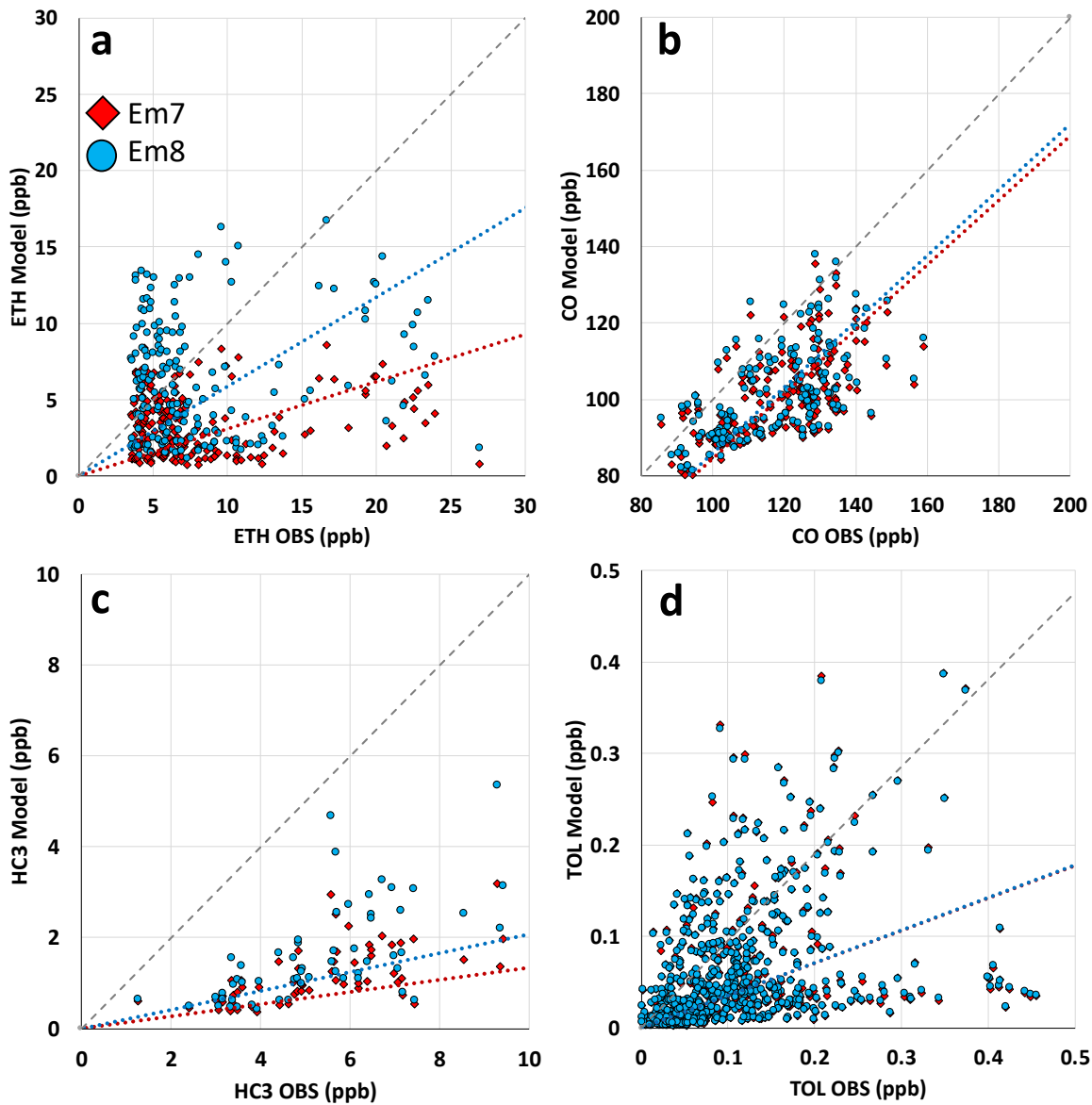
Figure 9. Scatter plot of measured vs. corresponding model values of ethane (a), CO (b), HC3 (c), and TOL (d) along the C130 PM flights limited to measurements in the NFR and below 2000m. Red diamonds represent the Em7 (base emissions) and blue circles represent Em8 (perturbed emissions). Red and Blue lines show the best fit using least square linear regression method for Em7 and Em8, respectively.
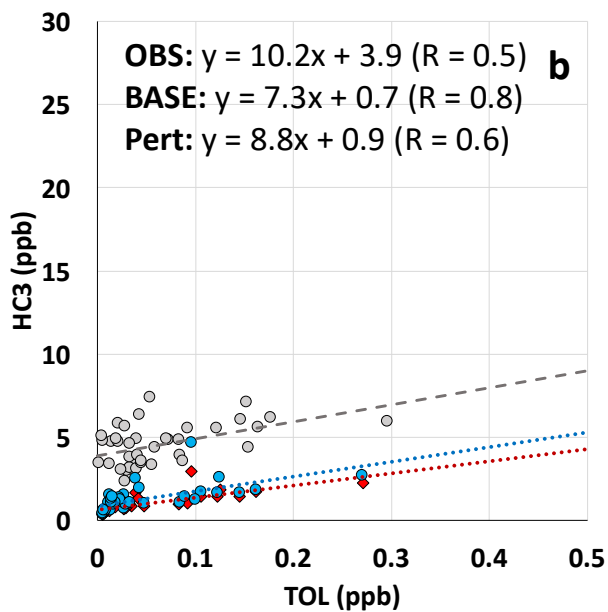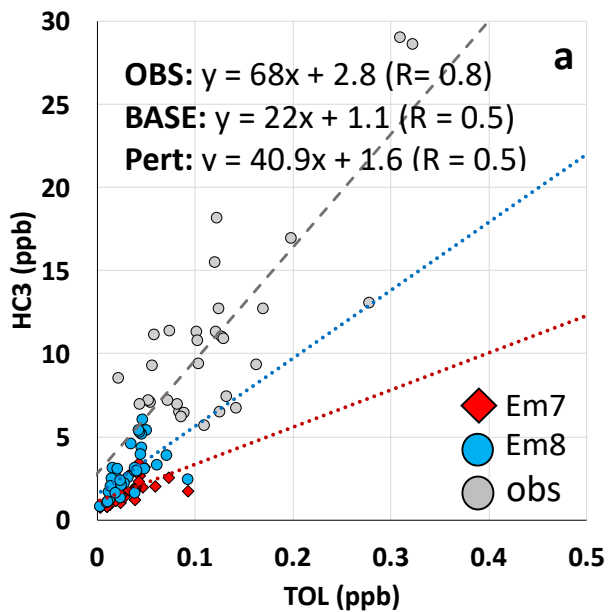
Figure 10. Sscatter plot of HC3 vs. TOL concentrations along the C130 PM flights limited to measurements in the NFR and below 2000m altitude. Plot (a) shows HC3 vs. TOL (when measured ethane is greater than 2ppb) for measurements and the corresponding model values. Plot (b) shows HC3 vs. TOL (when measured ethane is less than 2ppb) for measurements and the corresponding model values. Grey circles represent measurements, red diamonds represent the Em7 (base emissions), and blue circles represent Em8 (perturbed emissions). Grey, Red and Blue lines show the best fit using least square linear regression method for observations, Em7 and Em8, respectively.

List of Tables SM and Figures SM